Large-Scale Synthesis of Highly Luminescent InP@ZnS Quantum Dots Using Elemental Phosphorus Precursor

Eunbyul Bang

School of Energy and Chemical Engineering

(Chemical Engineering)

Graduate School of UNIST

Large-Scale Synthesis of Highly Luminescent InP@ZnS Quantum Dots Using Elemental Phosphorus Precursor

A thesis/dissertation
submitted to the Graduate School of UNIST
in partial fulfillment of the
requirements for the degree of
Master of Science

Eunbyul Bang

06. 15. 2017

Approved by

_____

Advisor

Jongnam Park

Large-Scale Synthesis of Highly Luminescent InP@ZnS Quantum Dots Using Elemental Phosphorus Precursor

Eunbyul Bang

This certifies that the thesis/dissertation of Eunbyul Bang is approved.

06. 15. 2017

Signature

_____

Advisor: Jongnam Park

Signature

_____

Jae Sung Son: Thesis Committee Member #1

Signature

_____

Hyesung Park: Thesis Committee Member #2

Signature

Abstract

Colloidal quantum dots can control the bandgap by controlling the particle size, and are capable of solution processing, which is cost competitive, and has a narrow half width of the emission wavelength. Using these characteristics, it is possible to utilize various kinds of LED, solar cell, and bio imaging. Among them, indium phosphide (InP) quantum dots have a bandgap capable of emitting light in the near-infrared region from the visible light region, and are less toxic to humans and the environment than cadmium-based quantum dots, and are attracting attention as next generation light emitting materials.

However, the limited choice and high cost of P precursors have a negative impact on their practical applicability. In this work, I report the large-scale synthesis of highly luminescent InP@ZnS QDs from an elemental P precursor (P_4), which was simply synthesized via the sublimation of red P powder. The size of the InP QDs was controlled by varying the reaction parameters such as the reaction time and temperature, and the type of In precursors. This way, the photoluminescence properties of the synthesized InP@ZnS QDs could be easily tuned across the entire visible range, while their quantum yield could be increased up to 60% via the optimization of reaction conditions. Furthermore, possible reaction pathways for the formation of InP QDs using the P_4 precursor have been investigated with nuclear magnetic resonance spectroscopy and it was demonstrated that the direct reaction of P_4 precursor with In precursor produces InP structures without the formation of intermediate species. The large-scale production of InP@ZnS QDs was demonstrated by yielding more than 6 g of QDs per one-batch reaction.

In the case of InP using different precursor P except the Tris(Trimethylsilyl) phosphine (($TMS)_3P$) there has been a problem that the size distribution is poor. Two kinds of P precursors with different reactivities were used to separate the nucleation and growth processes and to induce growth along the Lamer mechanism to produce uniform particles. For this, ($TMS)_3P$ and DEAP were used as fast reacting P precursors, and P_4 was used as a slow reacting P precursor. Through this, the possibility of uniform particle formation was observed. I strongly believe that the newly developed approach bears the potential to be widely used for manufacturing inexpensive high-quality QD emitters.

Contents

CHAPTER III: Synthesis of InP colloidal quantum dots with combined phosphorus sources

List of figures

Figure 1. Energy band structure of metal and semiconductor.

Figure 2. density states of semiconductor. (bulk:3D, Quantum layer:2D, Quantum wire:1D, Quantum dot:0D)

Figure 3. Concept of quantum confinement effect

Figure 4. Various types of core@shell structure

Figure 5. Various application for quantum dots; QD-LEDs/White LED, Solar cell, Bio-sensing.

Figure 6. Band gap energies and lattice parameters of various semiconductors.

Figure 7. a) Scheme for the synthesis of white P (P_4). b) Scheme for the further purification of white P.

Figure 8. ^{31}P-NMR spectrum of P_4 synthesized from red P. The inset indicates ^{31}P NMR spectrum of red phosphorus in the literature.

Figure 9. (a) Scheme for the synthesis of InP QDs using P4-TOP solution as P precursor. (b) UV−vis absorption spectra, (c) PL spectra, (d) time-resolved PL decays of InP@ZnS QDs with various sizes, and (e) photograph showing PL of InP@ZnS QDs solutions covering the entire visible ranges.

Figure 10. a) UV-Vis absorption spectra of InP QDs synthesized by varying [In/Zn] molar ratios at the reaction time of 30 min at 180 ℃. b) PL spectra of InP and InP@ZnS QDs.

Figure 11. a) Fitting of PL decays (black line) of InP@ZnS QDs with various sizes. PL decays of all types of InP@ZnS QDs were fitted by triexponential model. b) Log scale of PL decays of InP@ZnS QDs.

Figure 12. TEM images of a) red- and b) green-emitting InP@ZnS QDs. Size histograms of c) red- and d) green-emitting InP@ZnS QDs. e) XRD pattern of red-emitting InP@ZnS QDs. The vertical lines in a panel e indicate the XRD patterns of bulk InP (blue) and ZnS (red).

Figure 13. Low-magnification TEM images (500K) of a) green- and b) red –emitting InP@ZnS quantum dots to be used to estimate the size distribution of quantum dots.

Figure 14. a) Absorption spectra of InP cores b) PL spectra of InP@ZnS QDs using P_4 solution in tri-n-butylphosphine (TBP), oleylamine (OLA), and trioctylphosphine (TOP).

Figure 15. UV−vis absorption spectra indicating the effect of different reaction parameters on the size evolution of InP nanocrystals: a) temperature; b) indium halide precursor; c) OLA concentration; and d) amine chain length (OLA, HDA, DDA, and OTA indicate oleylamine, hexadecylamine, dodecylamine, and octylamine, respectively). Time-evolution absorption spectra of InP QDs synthesized from e) 180 ℃ and f) 210 ℃.

Figure 16. XPS spectra of InP quantum dots using $InCl_3$ and InI_3 precursors in the a) I 3d range and b) Cl 2p range.

Figure 17. a) UV-Vis absorption spectra of InP@ZnS QDs synthesized with $ZnCl_2$ and ZnI_2 additives.b) of InP core synthesized by varying In/P molar ratios.

Figure 18. PL spectra of InP@ZnS QDs synthesized by the single and double injections of P_4 precursors.

Figure 19. a) 31P NMR spectra of solutions of P4 in TOP, OLA, and the mixed solvent of TOP and OLA. b) 31P NMR spectra of the aliquots taken from the reaction mixture during the synthesis. c) Concentration profiles of P4 during the synthesis of InP.

Figure 20. a) Full-scale time-resolved ^{31}P-NMR spectra of the reaction solutions for the synthesis of InP QDs. b) The enlarged 31P-NMR spectra of TOP and solutions of P_4 in TOP, the mixed solvent of TOP and OLA.

Figure 21. a) Absorbance spectra of InP QDs with different type of solvents. b) Absorption spectrum of the product obtained with TOP as a P precursor and TOP+P_4 precursor.

Figure 22. (a) Photograph showing the amount of final product QDs obtained by a single-batch reaction. (b) UV−vis and PL spectra of corresponding InP@ZnS QDs. The inset shows the photograph of corresponding InP@ZnS QDs solution under UV irradiation.

Figure 23. Absorption peak change according to a) In / P ratio and b) OLA of InP synthesized with DEAP.

Figure 24. (a) Absorbance change according to the temperature of the InP core with $(TMS)_3P$ and P_4. (b) TEM of InP core synthesized using $(TMS)_3P$ and P_4 at 300 °C. (c) Absorbance change in the presence of P_4. (d) XRD data of InP core with only $(TMS)_3P$ and $(TMS)_3P + P_4$ combined phosphorus.

Figure 25. Absorbance change (a) in the amount DEAP with P_4, (b) in the amount DEAP only, (c) in the amount P_4, (d) in the amount TOP with DEAP.

List of tables

Chapter I. Introduction of Quantum dots and its application

1.1 Introduction of quantum dots

1.1.1 The definition of quantum dots

Quantum dots have been of great interest for fundamental study so that 14,000 papers are published during the past 30 years since they were first discovered. Quantum dots were first discovered by Dr. Louis Brus of Bell Laboratories and Dr. Alexei Ekimov of Russia for studying solar cells to overcome the energy in 1980's.[1]

When the size of materials is reduced to the size range of a few nanometers, the inherent energy state of the inorganic crystal changes to discontinuous, resulting in unique physical and chemical properties.[2] However, in the case of semiconductor materials, these characteristics are more evident. Because the Fermi level exists between the bands in the case of semiconductor quantum dots, the edges exist in a discontinuous energy state, which greatly affects the optical and electrical properties of the semiconductor materials. Therefore, the quantum dots are 0-dimensional semiconductor nanoparticles of several nanometers in size. When the radius of the nanocrystals is smaller than the exciton bore radius, electrons and holes are limited in movement and the energy level of a material has a discontinuous value for all directions. Due to the quantum confinement effect, the quantum dot is a material that emits light of various colors by itself without any device depending on the size of the nanocrystal.[3]

Figure 1 shows the density of states function in metals and semiconductors, showing that quantum dots are intermediates between atoms or molecules with discontinuous electron energy densities and bulk crystals with continuous energy bands. In other words, the optical and electrical properties of quantum dots are different from those of atoms, molecules, and bulk materials.[3]

Figure 2 shows the change in the density of states function of semiconductor material according to the dimension. Unlike bulk (3-D), film (2-D) and wire (1-D) materials, quantum dots (0-D) have the same density of states as the delta function. And the electrons and holes have a discontinuous energy state due to the limitation of their movement. Such quantum dots can be used in a variety of fields such as displays, solar cells, biosensors, and quantum computers in that they emit various high-purity light and excellent chemical properties.[3]
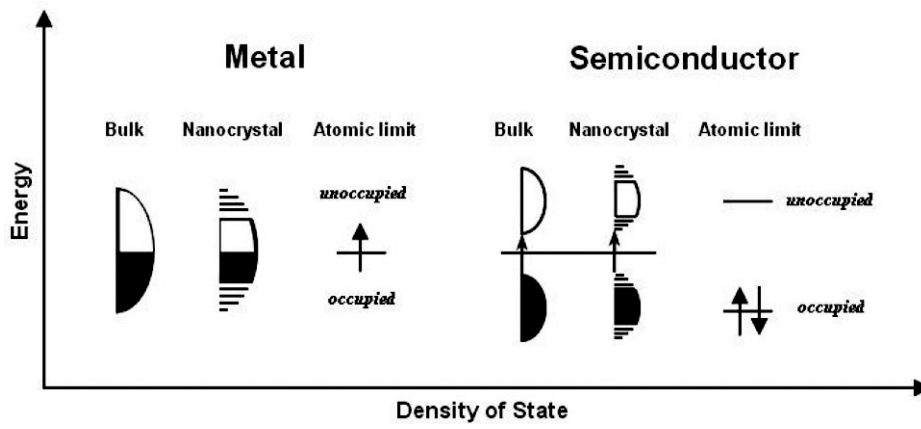
Figure 1. Energy band structure of metal and semiconductor.[3]
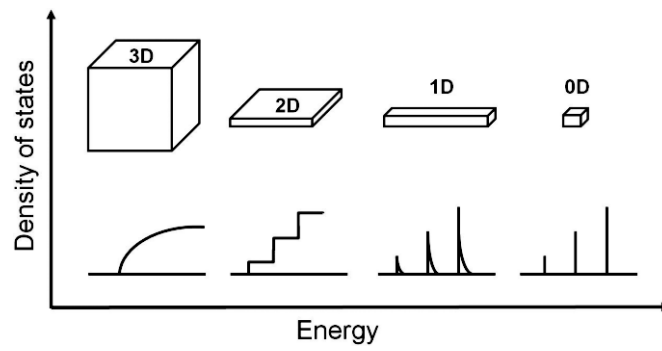
Figure 2. density states of semiconductor. (bulk:3D, Quantum layer:2D, Quantum wire:1D, Quantum dot:0D)[3]

1.1.2 Quantum confinement effect

When the radius of the semiconductor particles becomes smaller than the exciton bore radius, electrons and holes are spatially limited within the quantum dot, which causes discontinuous energy levels such as the energy state of the atom.[4] In the case of quantum dots having the same composition of semiconductor, the discontinuity of the energy level becomes larger as the size becomes smaller, and the bandgap of the quantum dot increases. The bandgap can also be explained by the following equation (1) by the particle in the box theory. The energies of a particle (En) is inversely proportional to the confinement distance of the particles (L). Therefore, the larger particle size, the smaller allowable energy difference of the particles. The quantum confinement effect is a phenomenon in which the band gap changes according to the size of the quantum dot.

$$E_n = \frac{n^2 h^2}{8mL^2} \ (n = 1, 2, 3 \ \cdots \ ) \ (1)$$

As the size of the quantum dot is reduced as shown in Figure 3[5], the semiconductor band gap is widened to absorb or emit light of a short wavelength. According to the quantum confinement effect, a large size quantum dot can absorb or emit light in near-infrared and visible light regions. By using this phenomenon, quantum dots can control the optical and electrical properties depending on the size.

Figure 3. Concept of quantum confinement effect[5]

1.2 Core@Shell structure of quantum dots

If the single core structure of the quantum dots is formed, the electric and optical properties of the quantum dots are deteriorated.[6] Because it acts as a trap site for electrons or holes and causes non-radiative reco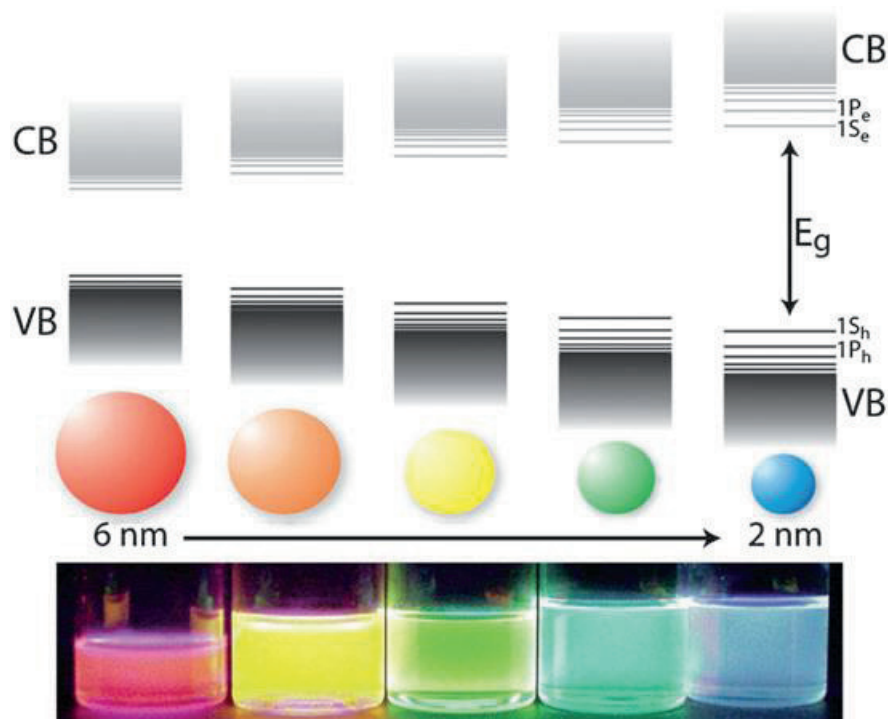mbination. To solve this problem, the Hines group reported for the first time how to stabilize the quantum dot itself by enclosing a shell of inorganic material in the core itself.[7] The core/shell structure has been studied as one of the methods for improving the stability and quantum efficiency of the quantum dots. The core/shell structure is divided into Type I and Type II as shown in Figure 5.

1.2.1 Type I of structure

In the Type I structure, the bandgap of the core is located between the bandgap of the shell, and electrons and holes existing in the core and shell are trapped inside the core. As a result, the recombination in the quantum dots having a core/shell structure is increased as compared with the quantum dots having only the core, leading to an increase in quantum efficiency. For example, a quantum well is formed by placing a CdSe (bandgap:1.74 eV) with a small bandgap on the core and a CdS (bandgap:2.42 eV) with a large band gap.[5] Since the CdSe surface is capped by CdS, the surface traps can be reduced and it is more stable than the CdSe single core quantum dot. At this time, the electrons are scattered throughout the quantum dot, but the holes are restricted to the cores only, so that photo-oxidation by the recombination of the hole-surface is prevented and stable fluorescence characteristics are exhibited. Since the quantum efficiency can be improved by increasing the recombination probability at the quantum dot, the quantum dot of such a structure is suitable for the light emitting diode device. As a typical example, CdSe / CdS, CdS / ZnS, CdSe / ZnSe, InP / ZnS and the like are known.[8,9]

1.2.2 Type II of structure

Type II structure is a structure in which the core band gap and the shell band gap are staggered by zigzag, and the location of trapping of electrons and holes depends on the thickness of the shell and the position of the band gap. If the conduction band and the valence band of the core are lower or higher than the shell, the lifetime of the excitons is lengthened. So that electrons and holes are spatially separated between the core and the shell in a low energy state before recombination. Type II structures are limited to the core/shell, respectively, so that radiative recombination occurs at the interface of the core/shell. When two or more semiconductor materials are formed in this manner, the portion having a

small difference in bandgap serves as a bandgap of the core/shell. This structure causes a considerable long wavelength shift depending on the thickness of the shell. In addition, as the thickness of the shell increases, electrons and holes are also present in the outer shell, so that quantum efficiency and optical stability can be expected as with type I. Another advantage of this structure is that the decay time of the fluorescence is increased because the electron and hole are separated and the overlap of the wave function is reduced. This is suitable for photovoltaic devices such as solar cells because it is advantageous to extract electrons by separating electrons and holes from each other.[9]
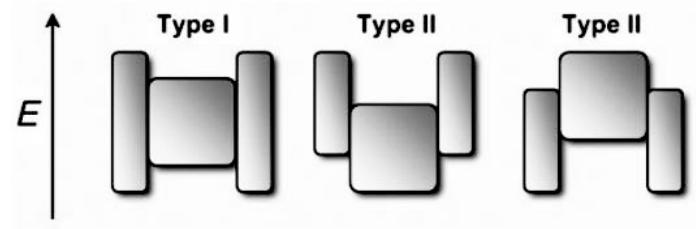
Figure 4. Various types of core@shell structure[6]

1.3 Application for quantum dots

The quantum dot can realize the light of the entire visible region through the quantum confinement effect. As shown in Figure 6, research is being actively carried out in LED, laser beam, solar cell and bio field.[10-15] In the field of solar cell, the quantum dot solar cell is a concept that can overcome the theoretical limit of the previous solar cell. Compound semiconductor quantum dot solar cells can be applied to satellite, military, and condensing type of solar cells. The quantum dot solar cell can be controlled to absorb light of a specific wavelength by the quantum confinement effect. In other words, if one solar cell is combined with quantum dots of different sizes, it is possible to cover the whole solar spectrum, and thus it is expected that the efficiency can be enhanced as compared with a general bulk compound semiconductor.

The LED market is expected to form a huge component and materials market that surpasses the semiconductor market in the future. Because it spans all industries as well as display devices such as a mobile phone, a PDA, a digital camera, a computer, a television. LED are attracting attention as display devices that can solve the limitations of conventional LCD such as backlight requirement, high power consumption, slow response speed. In the field of LEDs, the colloidal quantum dot has excellent luminescence characteristics (high color purity, high luminescence efficiency, and various emission bands), and a new display device can be realized by using quantum dots. Actually, such as OLED properties, the quantum dots can emit light themselves are similar, but it can create even smaller pixels to implement an improved color sharpness. In addition, because it is produced by printing method, it can be enlarged, folded and folded, and it is emerging as a next generation display that surpasses conventional LCD. MIT and QD Vision have developed light emitting diodes using the electroluminescence properties of quantum dots. For the application of quantum dot light-emitting devices, the development of non-toxic environmentally friendly quantum dots containing no heavy metals such as Cd, Hg and Pb, study of optical properties of quantum dots, and development such as nano patterning technology are needed.

Finally, observing molecules or cells through fluorescent probes in the field of biotechnology is now widely used as an important technology for revealing biological mechanisms. Since the size range of quantum dots is similar to that of functional biomaterials, biocompatible nanoparticles can predict breakthroughs in biological and medical applications.
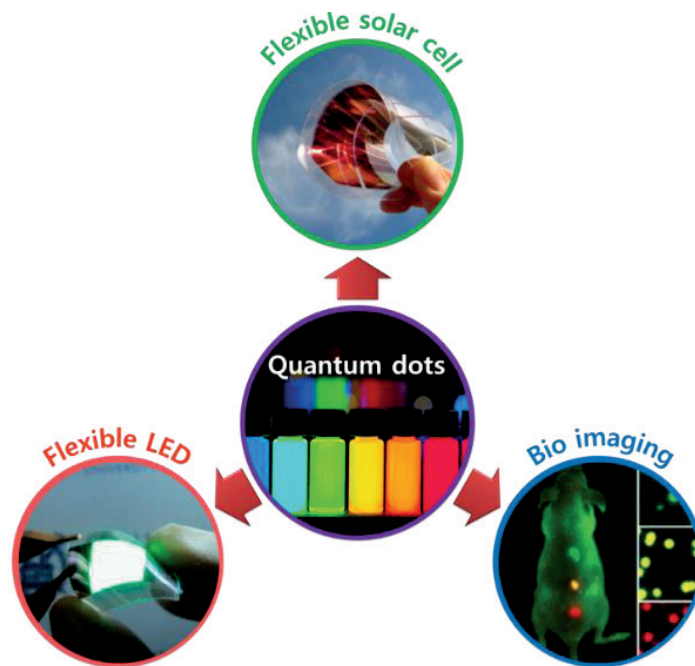
Figure 5. Various application for quantum dots; QD-LEDs/White LED, Solar cell, Bio-sensing.[10-15]

.

1.4 Semiconductor nanocrystals

Most of the quantum dot materials consist of II-VI group and III-V group compound semiconductor. CdSe, CdS, CdTe, ZnS, and ZnSe is example of II-VI group compound semiconductor.[16] Although it has high luminescence efficiency and optical stability, recently human hazard has been raised as a problem. III-V group are typically InP quantum dots. InP are the most widely studied quantum dots due to their non - toxic nature and their broad emission range similar to CdSe quantum dots. However, since the luminescence efficiency is lower than that of the II-VI group quantum dots and InP has a relatively wide full width half maximum (FWHM) value, research is needed to overcome these problems.[17] As shown in Figure 6, CdSe and InP quantum dots, especially among various kinds of quantum dots, are suitable quantum dots for display applications because they can control the size to a desired wavelength in the entire visible light.

1.4.1. II-VI group quantum dots

The II-VI group quantum dots have been studied extensively as a material capable of emitting light with high luminescence efficiency, optical stability. Among the II-VI group, the CdSe quantum dot is a direct bandgap of 1.74 eV and can emit light with high luminous efficiency, optical stability, and full viewing range. In the CdSe quantum dot synthesis, the properties of the quantum dots depend on various conditions such as reaction temperature, reaction time, precursor concentration and pH.[18] The main determinant factor of nucleation and growth on CdSe quantum dots is the reaction temperature. Although $Cd(CH_3)_2$ was mainly used for the initial CdSe quantum dot synthesis, $Cd(CH_3)_2$ is highly toxic at room temperature and chemically unstable. Furthermore, when the temperature rises, it becomes explosive and is very dangerous. For this reason, the synthesis method using $Cd(CH_3)_2$ can be synthesized only under limited equipment and conditions, and is unsuitable for making large quantum dots. In the Pengs group, cadmium salt and cadmium acetate such as CdO and Cadmium carbonate were used as substitutes for the Cd precursor.[19]

1.4.2. III-V group quantum dots

Typical II-VI group semiconductor have received much attention due to their advantages such as high luminescence efficiency and stability, and much research have been studied. However, not only does Cd^{2+} and Se^{2-} contain harmful substances, but it also causes serious problems and may have harmful effects on the human body when applied to the biotechnology field.[17] In order to solve this problem, a

large number of III-V binary and I-III-VI ternary compound semiconductor quantum dots, which can replace II-VI series quantum dots, have been studied. Of the III-V group quantum dots, the InP quantum dot are the most extensively studied materials due to their non-toxicity advantages compared with the II-VI compound semiconductors, their luminescent area similar to the CdSe quantum dots, and good luminescence efficiency. InP quantum dot are representative III-V group quantum dot having a wide emission range from the visible light to the near infrared region. In general, however, InP quantum dots exhibit inferior quantum yield and relatively broad emission FWHM values as compared with the II-VI group quantum dots. For this reason, many studies have been conducted to synthesize InP quantum dots having improved luminescence efficiency.

1.4.3. I-III-VI group quantum dots

I-III-VI group quantum dot have recently attracted attention as bio- and medical applications due to their non-toxicity and environmental harmlessness, as well as III-V series quantum dot. Typical examples include $CuInSe_2$(CISe), $CuInS_2$(CIS) and $AgInS_2$(AIS).[20,21] Among them, CIS, which is a direct bandgap semiconductor, has a band gap of 1.5 eV and its absorption characteristic is similar to the sunlight spectrum. In addition, the CIS quantum dot is suitable for bio applications due to their stability, and they are actively studied due to the relatively non-toxic characteristics of CISe quantum dot.
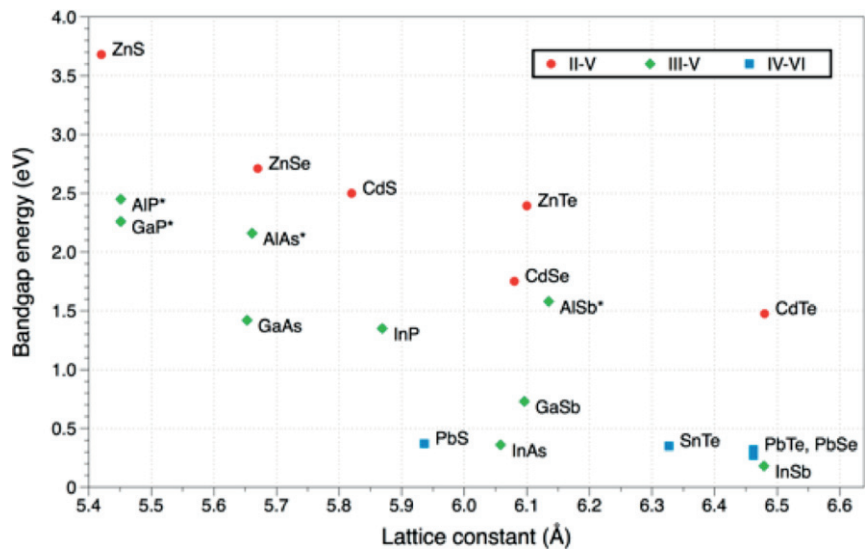
Figure 6. Band gap energies and lattice parameters of various semiconductors.[17]

1.5 Indium Phosphide Quantum Dots

1.5.1   Basic properties of InP QDs

InP, which is a representative III-V semiconductor, is a direct band gap semiconductor like CdSe, and it emits light by recombination of excitons excited by external light. Therefore, it has narrow visible light emission linewidth among non-Cd type quantum dots, and is becoming a subject of more intensive research and development. InP is a zinc blende structure at room temperature and has a band gap of 1.35 eV for bulk crystals and has a bore radius of about 15 nm. Therefore, it is possible to expand band gap and discontinuous band gap at sizes below 10 nm. InP quantum dots can control the emission spectrum from the near-infrared region to the visible region (green) through particle size control. The synthesis of InP quantum dots is mainly performed by a hot injection method like the conventional CdSe. In this method, a precursor mixture at room temperature is injected into a high-temperature medium containing a surfactant. However, because of the nature of covalent InP, it is not easy to synthesize. Tris(trimethylsilyl)phosphine [(TMS)$_3$P], which is used in most synthetic processes, requires a great deal of caution in handling it as a flammable compound that is harmful to the human body.[17]

1.5.2 history of InP QDs

The synthesis of InP with zinc blende crystal structure was the first colloidal synthesis using the oxalate complex of indium chloride (prepared by the reaction of indium trichloride and sodium oxalte) and TMSP as indium precursor and phosphorus sources, respectively. In this study, trioctylphosphine oxide and trioctylphosphine were used together to enhance the stability, and the reaction was carried out at 270 ° C for 3 days.[ref] X-ray diffraction and high-resolution TEM were used to reveal that it has a zinc blende crystal structure and an ellipsoidal shape. InP was synthesized by varying the In: P ratio in order to optimize QD characteristics. The narrowest particle size distribution was obtained from excess indium. However, the emission spectrum occurred in two bands. On the other hand, when phosphorus was added excessively, it had a wide size distribution. Despite such a long time of three days, it showed a broad size distribution and had to undergo a size selction process after synthesis. In order to synthesize satisfactory quality InP nanocrystals without additional selction process, it is

important to control the conditions of the proper coordinating and noncoordinating solvents, strict ratio control of indium and ligand, and reaction mixture.

Subsequently, peng et al. first succeeded in synthesizing high-quality InP QDs by using fatty acids such as 1-octadecene, noncoordinating solvents and different chain lengths, amines, phosphines, and phosphonic acids as capping ligands.[22] Indium acetate (In(Ac)$_3$) and P(TMS)$_3$ were used as precursors. Now, the best results were obtained when the indium: phosphorus ratio was 2:1, and all the synthesized nanocrystals were dissolved in a general polar solvent. Also, when fatty ligands such as palmitic acid and myristic acid were used, the best results were obtained under the conditions using ODE. This method has an elongated shape, and the QY of 3 nm size does not exceed 5%, but it was a breakthrough. Compared to the conventional method, which took several days, it could be synthesized in a few hours, the particles obtained had a narrow size distribution, and the particle size could be adjusted.

Today, most of the InP NCs synthesis methods using P(TMS)$_3$ use 1-octadecene with indium precursors and stabilizing ligands such as fatty acids, amines or alkylphosphines. This method relies on an expensive TMSP precursor as a phosphorus precursor, which performs a hampering scale-up of the synthesis. In(tBu$_2$P)$_3$,[23] Na$_3$P,[24] Ca$_3$P,[25] PCl$_3$[26] and as well as white phosphorus(P$_4$)[27] have been studied as alternative phosphorus precursors for phosphorus precursors which are less costly in synthesis and less toxic.

Chapter II. Synthesis of InP colloidal quantum dots with white phosphorus for new phosphine precursor

2.1 Introduction

Colloidal semiconductor quantum dots (QDs) have attracted considerable attention in various disciplines due to their unique size- and shape-dependent optical and electronic properties.[28-34] In particular, their light-emitting characteristics in a wide range of wavelengths, i.e., from ultraviolet to near-infrared, makes them a new class of emitters for various technological applications such as light-emitting diodes, lasers, and biomedical imaging.[35-41] As of today, various semiconductors (including the II−VI[42-45] and III−V[46-48] families) have been suggested for such uses, and InP QDs can be recognized as important candidates for cd-free environmentally benign emitters, operating across the entire visible range. However, despite the recent efforts to synthesize high-quality InP QDs, reliable protocols are still required for realizing their reproducible size control, narrow size distribution, and large-scale production. In fact, manufacturing of these QDs is negatively affected by the limited choice and high cost of P precursors, which must possess sufficient reactivity to overcome the covalent nature of the In−P bond.[49-51]

The reactivity of P precursors strongly depends on the energy of their P−X bonds (X = Si, Ge, or N). Since Wells et al. have first reported a dehalosilylation reaction of an indium halide salt with tris(trimethylsilyl)phosphine ($P(TMS)_3$),[52] tris(trialkylsilyl)phosphine represents the most widely used P precursor with a relatively low P−Si bond dissociation energy (around 363 kJ/mol),[53] which leads to its high reactivity during the reaction with an In precursor. At the same time, such a high reactivity of P precursors sometimes results in their fast depletion at high temperatures,[54,55] which makes the control of the formation and growth of the resulting InP QDs very difficult. Furthermore, it restricts the large-scale production of InP QDs due to its sensitivity to temperature homogeneity of the reaction batch. Thus, there have been significant research efforts to develop alternative P precursors such as Na_3P,[24] Ca_3P,[25] and PCl_3,[26] as well as P_4[56,57]. P is one of the relatively abundant elements and typically exists as a phosphate form, which is converted industrially to elemental P, such as white P (P_4) and red P allotropes.[58-60] Red P is considered the most common P allotrope and can be transformed to P_4, which is the most reactive P allotrope. Also, P_4 exhibits the moderately high bond dissociation energy of 460 kJ/mol of the P−P bond in P_4[53] and thus has been extensively utilized for designing P-containing transition metal complexes. Recently, several attempts have been made to use P_4 and related compounds as precursors for the synthesis of InP QDs via solvothermal reactions.[56,57] For example, Xie et al. reported the solvothermal synthesis of InP nanocrystals using P_4 precursor in the presence of the reducing agent KBH_4.[56] The size of synthesized nanocrystals was in the range of

11−20 nm, and, further, nanorods with a diameter of 150 nm were produced. Mézailles et al. synthesized InP QDs with diameters of 2−10 nm via the reaction of P_4 with preformed In nanoparticles.[57] However, all these approaches were unable to provide a reliable synthesis route for monodispersed and highly luminescent InP-based QDs. In this work, I developed a synthesis of InP and InP@ZnS QDs using P_4 as a P precursor, which had been simply synthesized from red P powder. The luminescence colors of InP@ZnS QDs were easily tuned from blue (480 nm) to red (630 nm) by controlling their sizes. In particular, the optimized synthesis condition increased the quantum yield (QY) of InP@ZnS QDs to 60%. In addition, possible reaction pathways for the formation of InP QDs were studied with ^{31}P nuclear magnetic resonance (^{31}P NMR) technique. Finally, I demonstrate that our synthesis approach allows large-scale production of InP@ZnS. This new type P precursor will enrich the chemistry for the synthesis of various metal phosphide nanocrystals. Moreover, I believe that our approach will provide a great potential for various applications of InP QDs as economic and high-quality emitters.

2.2 Experimental session

2.2.1 Materials

Indium(III) chloride (99.999%), zinc(II) chloride (98+ %), indium(III) iodide (99.998%), zinc(II) iodide (98+%), oleylamine (OLA, 98+%), hexadecylamine (HDA, 98%), dodecylamine (DDA, 99%), octylamine (OTA, 99%), tri-n-octylphosphine (TOP, 97%), tri-n-butylphosphine (TBP, 97%), zinc acetate (99.99%), oleic acid (90%), 1-octadecene (ODE, technical grade, 90%), and 1-dodeca-nethiol (98+%) were purchased from Sigma-Aldrich. Phosphorus powder (98.9%) was purchased from Alfa Aesar. Chloroform-D1 was purchased from Merck Millipore. All chemicals above were used directly without any purification.

2.2.2 Synthesis of White P (P$_4$).

First, 35 g of amorphous red P powder was put into an Erlenmeyer flask. The Erlenmeyer flask was connected with a 250 mL round-bottom flask using a U-shaped connector (Figure 7a). In order to capture vaporized P$_4$, the round-bottom flask was lowered into a cooling bath containing a mixture of acetone and dry ice. The red P was heated to 350 °C with a heating rate of 6 °C/min under vacuum and maintained at this temperature for at least 4 h. At this stage, the obtained P was a mixture of red P and P$_4$. For further purification, the obtained product was sublimated using a sublimator kit and heated slowly to 100 °C under vacuum (Figure 7b). This sublimation process was performed thrice to improve the purity of P$_4$. The finally obtained P$_4$ was a lump-like solid with a weight of ～28 g, and the chemical yield was ～80%. The purity of the synthesized P$_4$ was confirmed by ^{31}P NMR spectroscopy analysis (Figure 8). The ^{31}P NMR spectrum shows a single peak that can be assigned to P$_4$. In particular, no peaks related to red P were detected. *Caution!* P$_4$ spontaneously ignites when it is exposed to the air. Therefore, all synthetic processes to produce P$_4$ must be carried out in a glovebox under inert atmosphere. Additionally, the synthesized P$_4$ should be stored in the dark (in the glovebox) since P$_4$ transforms slowly to yellow P when exposed to light.

2.2.3 Synthesis of Blue-Emitting InP@ZnS QDs

A 148.7 mg amount of indium iodide and 469.2 mg of zinc iodide were dissolved in 3.3 mL of OLA in a 50 mL three-neck flask. This solution was degassed at 120 °C for 1 h and then heated to 180 °C under inert atmosphere. A 37 mg amount of P$_4$ powder was dissolved into TOP at 80 °C for

several hours. Subsequently, the solution was injected into the reaction mixture, which was kept at that temperature for 30 min. For coating the ZnS shell, the previously prepared InP core solution was heated to 210 °C. Then, 4 mL of zinc oleate (1.376 g of zinc acetate was dissolved in 4.75 mL of oleic acid at 120 °C under Ar atmosphere and diluted with 10.25 mL of ODE) was added into the InP core solution. After 1 min, 1.8 mL of 1-dodecanethiol was injected into the solution and the reaction was maintained for 90 min. The solution was then cooled to room temperature and precipitated with the addition of mixed nonsolvents of 20 mL of acetone, 10 mL of 1-butanol, and 20 mL of ethanol. The mixture was subsequently centrifuged at 5000 rpm for 5 min. The final product was re-dispersed in hexane.

2.2.4 Synthesis of Green-Emitting InP@ZnS QDs.

A 66.4 mg amount of indium chloride and 200.4 mg of zinc chloride were dissolved in 3.3 mL of OLA in a 50 mL three-neck flask. This solution was degassed at 120 °C for 1 h and then heated to 150 °C under inert atmosphere. A 2 mL aliquot of P_4-TOP solution containing 56 mg of P_4 was injected into the reaction mixture which was kept at that temperature for 30 min. For coating the ZnS shell, the reaction method and conditions were the same as above.

2.2.5 Synthesis of Yellow-Emitting InP@ZnS QDs

A 66.4 mg amount of indium chloride and 200.4 mg of zinc chloride were dissolved in 3.3 mL of OLA in a 50 mL three-neck flask. This solution was degassed at 120 °C for 1 h and then heated to 180 °C under inert atmosphere. A 2 mL aliquot of P_4-TOP solution containing 56 mg of P_4 was injected into the reaction mixture which was kept at that temperature for 30 min. For coating the ZnS shell, the reaction method and conditions were the same as above.

2.2.6 Synthesis of Orange -Emitting InP@ZnS QDs.

A 66.4 mg amount of indium chloride and 200.4 mg of zinc chloride were dissolved in 1.65 mL of OLA in a 50 mL three-neck flask. This solution was degassed at 120 °C for 1 h and then heated to 180 °C under inert atmosphere. A 2 mL aliquot of P_4-TOP solution containing 56 mg of P_4 was injected into the reaction mixture which was kept at that temperature for 30 min. For coating the ZnS shell, the reaction method and conditions were the same as above.

2.2.7 Synthesis of Red-Emitting InP@ZnS QDs

A 66.4 mg amount of indium chloride and 200.4 mg of zinc chloride were dissolved in 1.65 mL of OLA in a 50 mL three-neck flask. This solution was degassed at 120 °C for 1 h and then heated to 210 °C under inert atmosphere. A 1.1 mL aliquot of P_4-TOP solution containing 31 mg of P_4 was injected into the reaction mixture which was kept at that temperature for 10 min. Then, the secondary injection of 0.9 mL of P_4-TOP solution containing 25 mg of P_4 was performed for the further growth of InP QDs. As before, the reaction mixture was kept at a temperature of 210 °C for 10 min. For coating the ZnS shell, the reaction method and conditions were the same as above.

2.2.8 Optical Properties

Absorption spectra were recorded with a Shimadzu UV-1800 UV−visible spectrometer. Photoluminescence (PL) spectra were taken with an Agilent FL 1004 M008. Measure-ments for nanocrystal solutions were performed for each sample at room temperature. Time-resolved PL (TRPL) measurements were performed with a time-correlated single-photon counting setup (FluoTime 300, PicoQuant) at room temperature. The QD samples were diluted in hexane solution and excited by a 450 and 510 nm CW and pulsed diode laser head (LDH-D-C 450 and LDH-D-C 510) coupled with a laser diode driver (PDL 820, PicoQuant) and a repetition rate of between 196 kHz and 40 MHz. The peak photon count was set to 10000 for all measurements. The PL lifetime (τ) was obtained by fitting the decay curve with a triexponential decay function. PL QY of InP@ZnS QDs synthesized from P4 was obtained by comparing PL intensities between primary dye solution and InP@ZnS QDs at the same excitation wavelength. For example, in the case of InP@ZnS with emission wavelength of 530 nm, Coumarin 545 was used as a primary dye solution and PL intensity was measured at 484 nm excitation wavelength. The relative PL QY of QDs was calculated by the following equation.

$$\text{PL QY} = 0.95 \times \frac{I_{QD}}{I_{dye}} \times \frac{A_{dye}}{A_{QD}} \times \frac{nhexane_2}{nethanol_2} \qquad (1)$$

In this equation, I is the integrated area of a PL spectrum, A is the absorbance of a solution at excitation wavelength, and n is the refractive index of the solvent used. Rhodamine 101, Rhodamine 6G, and Coumarin 545 were used as a primary dye solution, depending on their PL wavelengths. The measurements of PL QY and full-width at half-maximum (fwhm) were conducted on more than five sets of samples exhibiting PL at 480, 530, 560, 600, and 630 nm, respectively. The results with standard error are summarized in Table 1.

2.2.9 Nuclear Magnetic Resonance Analysis.

All NMR tubes were baked at 120 °C overnight and transferred to a glovebox before used. TOP (300 μL) was mixed with chloroform-D1 (300 μL). P_4 (0.05 g) was melted at 80 °C and mixed with chloroform-D1 (500 μL). P_4 (0.05 g) and TOP (2 mL) was mixed at 80 °C, and 300 μL of P_4-TOP solution was mixed with chloroform-D1 (300 μL). P_4 (0.05 g), TOP (2 mL), and OLA (2 mL) was mixed at 80 °C and 300 μL of P_4-TOP-OLA solution was mixed with chloroform-D1 (300 μL). All mixtures were transferred to NMR tubes inside the glovebox and used for ^{31}P NMR spectroscopy. For the time-evolution measurement of reaction solutions, 1, 3, 10, and 30 min aliquots (300 μL) were taken from the reaction mixture during the synthesis of InP QDs at 180 °C after the injection of P_4-TOP solution and immediately mixed with chloroform-D1 (300 μL).

2.2.10 Transmission Electron Microscopy.

Transmission electron microscopy (TEM) and HRTEM images were taken with a JEOL JEM-2100 microscope with an acceleration voltage of 200 kV using copper grids (Ted Pella, USA). The hexane solutions containing nanocrystals were deposited on the copper grids.

2.2.11 X-ray Powder Diffraction.

X-ray powder diffraction (XRD) measurements were carried out with a Rigaku Ultimate-IV X-ray diffractometer operated at 40 kV/200 mA using the Cu Kα line (λ=1.5418 A). Nanocrystal powder samples were placed onto glass substrates after purification by the standard precipitation procedure with hexane as the solvent and acetone and ethanol as precipitation reagents.

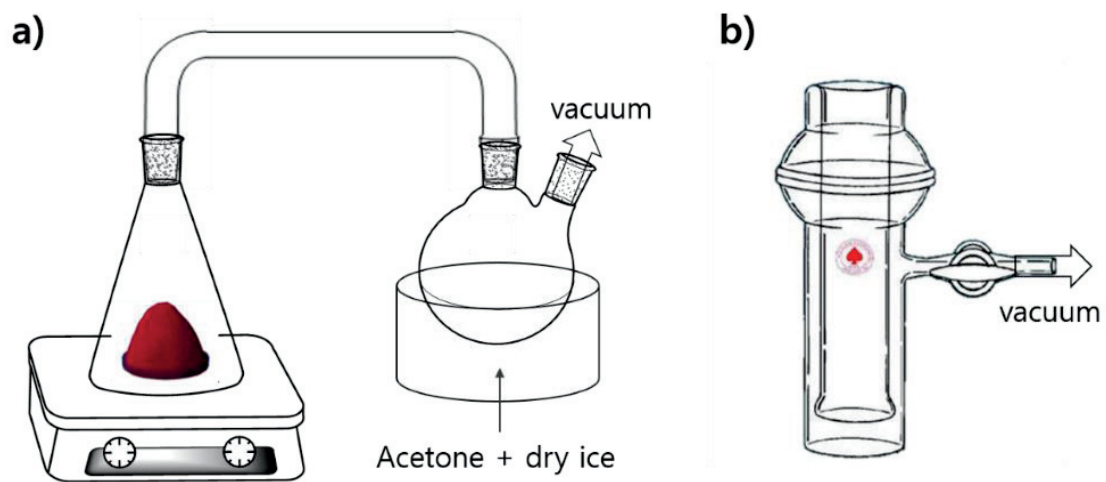**Figure 7.** a) Scheme for the synthesis of white P (P_4). b) Scheme for the further purification of white P.
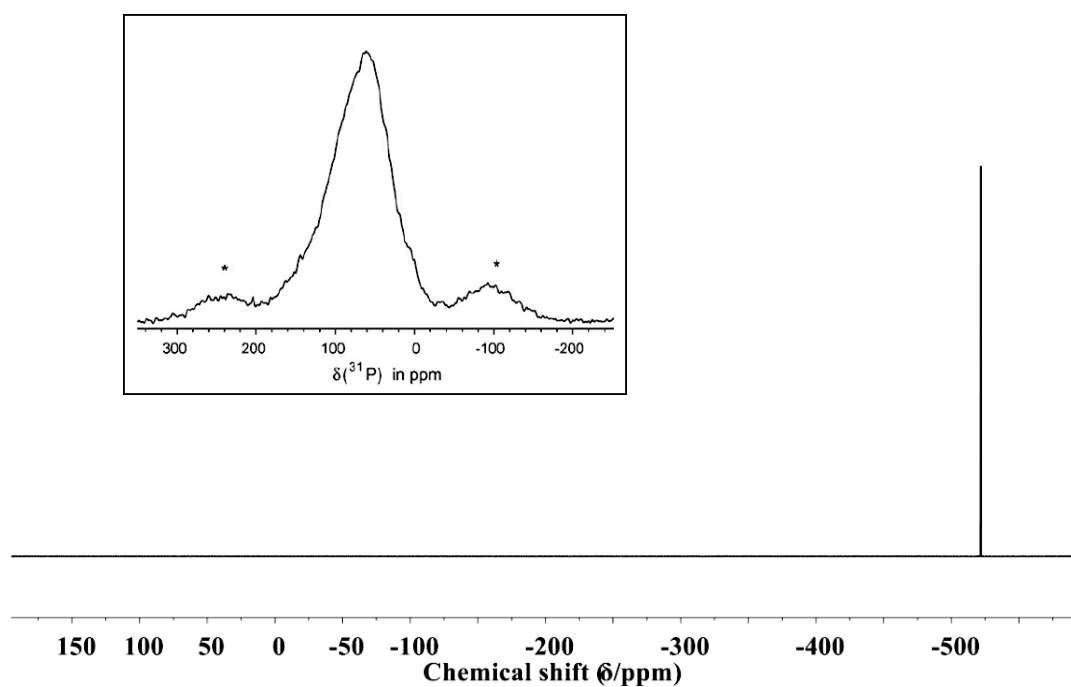
Figure 8. ^{31}P-NMR spectrum of P_4 synthesized from red P. The inset indicates ^{31}P NMR spectrum of red phosphorus in the literature.

Table 1. QY and FWHM of InP@ZnS QDs.

QD PL peak (nm)	482±1	529±2	555±2	595±2	635±3
QY (%)	8±2	60±2	60±1	40±3	18±2
fwhm (nm)	58±1	63±1	69±2	77±1	76±1

2.3 Result & Discussion

2.3.1 Synthesis and Optical Properties of InP quantum dots using P_4 precursor

InP QDs were synthesized from newly developed elemental P precursor solution. Red P powder was sublimated to obtain P_4, and subsequently, it was dissolved in TOP by stirring at a moderate temperature of 80 °C (Figure 9a). The resulting P_4 solution in TOP was then injected into a solution of indium halide in oleylamine in the presence of Zn halides at a specified temperature (Figure 9a). OLA served both as a solvent and as a source of ligands for the resulting nanocrystals.[61-63] It is well-known that Zn^{2+} ions effectively passivate the growth of InP QDs without diffusing into the InP lattice, thus improving the QD size distribution (Figure 10a).[64,65] To synthesize InP@ZnS QDs, zinc oleate and 1-dodecanethiol were subsequently added into the reaction mixture and aged. The ZnS shell coating significantly improved the photoluminescence (PL) properties of the QDs (Figure 10b).

The absorption and PL spectra were measured for the synthesized InP@ZnS core@shell QDs over the entire visible range (Figure 9b,c). The absorption spectrum of InP@ZnS QDs shows the distinct first excitonic transition, indicating a narrow size distribution of the nanocrystal ensembles. Furthermore, the first excitonic transition peak in the absorption spectrum of InP@ZnS core@shell QDs was precisely tuned from 424 to 589 nm, showing the wide range of achievable sizes. This size control was best demonstrated by the tuning of the emission color of InP@ZnS QDs from blue to red (Figure 9c,e), as shown in the PL spectrum tuned from 480 to 630 nm. The QY of green- and yellow-emissive InP@ZnS QDs was reproducibly increased up to a magnitude of 60% and more (Table 1).

The fact that the blue-, orange-, and red-emitting QDs exhibited a lower QY than the green- and yellow-emitting ones (Table 1) is in line with various previous studies, where InP@ZnS QDs were synthesized using $P(TMS)_3$, and which report that the highest QY was achieved in green- and yellow-emitting QDs. Furthermore, with our results, I demonstrate for the first time the synthesis of highly luminescent InP-based QDs by using a P_4 precursor, which exhibit a QY that can compete with the QY of InP@ZnS QDs synthesized by using $P(TMS)_3$. The full width at half-maximum of the PL peak of InP@ZnS QDs was in the range from 50 to 80 nm and increased with increasing wavelength of the PL peak (Table 1).

TRPL measurements were performed for InP@ZnS QDs with various sizes to investigate the PL decay kinetics (Figure 9d), and the obtained data were analyzed using a triexponential model depending on the type of indium halide precursor (Figure 11). The average PL decay times measured for the red-, orange-, yellow-, and green-emitting QDs (synthesized using $InCl_3$ as the In precursor) were around 55−58 ns, which was comparable to the reported values for InP@ZnS QDs[66] and larger than the value of ~22 ns obtained for the blue-emitting QDs synthesized from InI_3 (Table 2). It is

interesting to note that the portion of the fastest exciton decay component ($\sim$3.5 ns) in the blue-emitting QDs was much higher than in the other InP@ZnS QDs. Since the decay time is very sensitive to the surface passivation of QDs due to the recombination of excitons in the internal core state, this phenomenon may originate from surface defects of blue-emitting QDs, synthesized from InI_3.[67,68] The steric hindrance effect of I^- ions partially capping InP QDs may slow the surface reaction rate for the ZnS shell coating and form surface defects.[62] In fact, typical InP core QDs without inorganic shell coating are known to exhibit exciton decay times in the order of several nanoseconds, which is comparable to that of the current blue-emitting InP@ZnS QDs.[69,70] This phenomenon was further reflected by the relative low QY of blue-emitting InP@ZnS QDs because the QY strongly depends on the degree of surface passivation (Table 1).
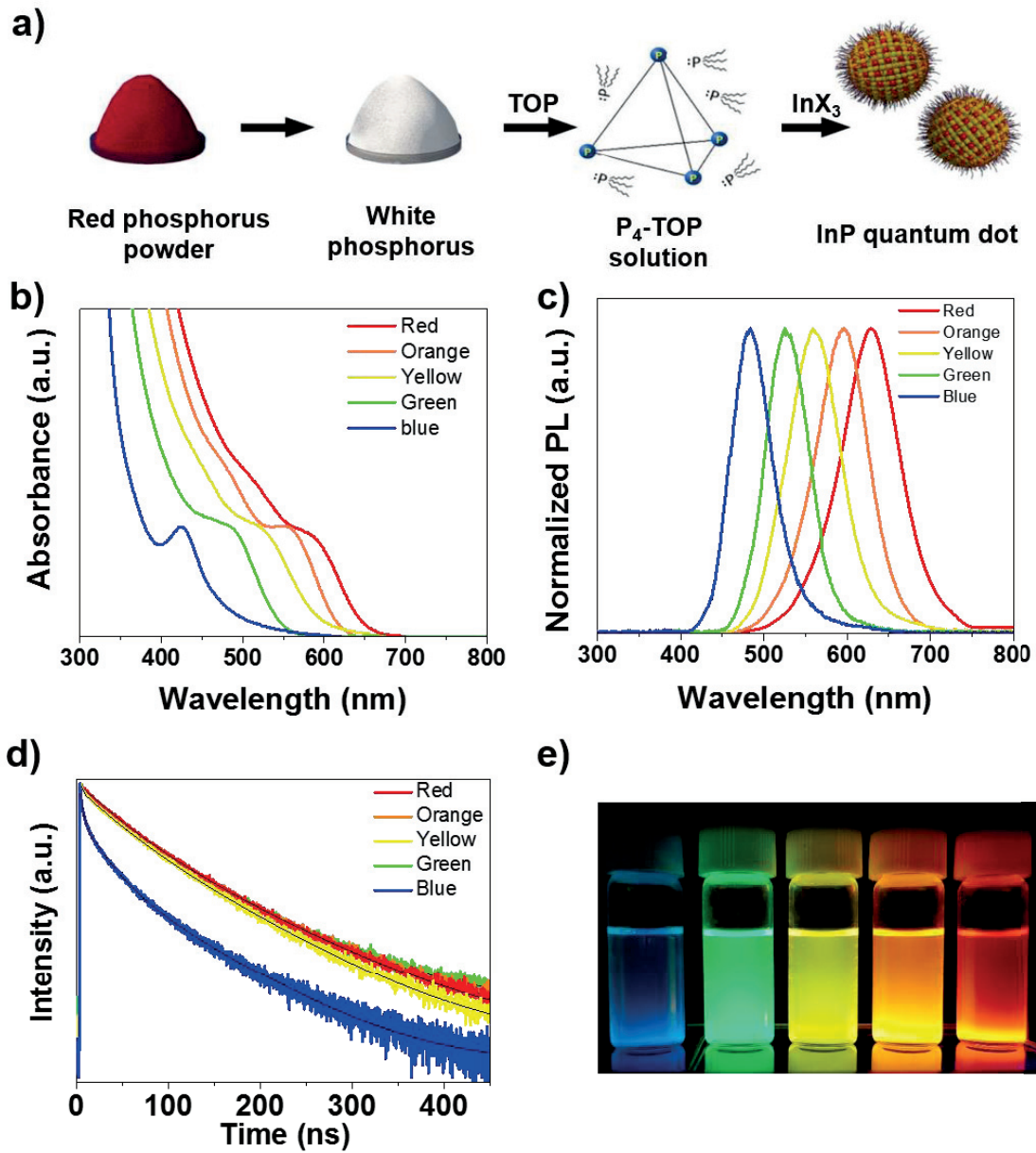
Figure 9. a) Scheme for the synthesis of InP QDs using P4-TOP solution as P precursor. b) UV−vis absorption spectra, c) PL spectra, d) time-resolved PL decays of InP@ZnS QDs with various sizes, and e) photograph showing PL of InP@ZnS QDs solutions covering the entire visible ranges.
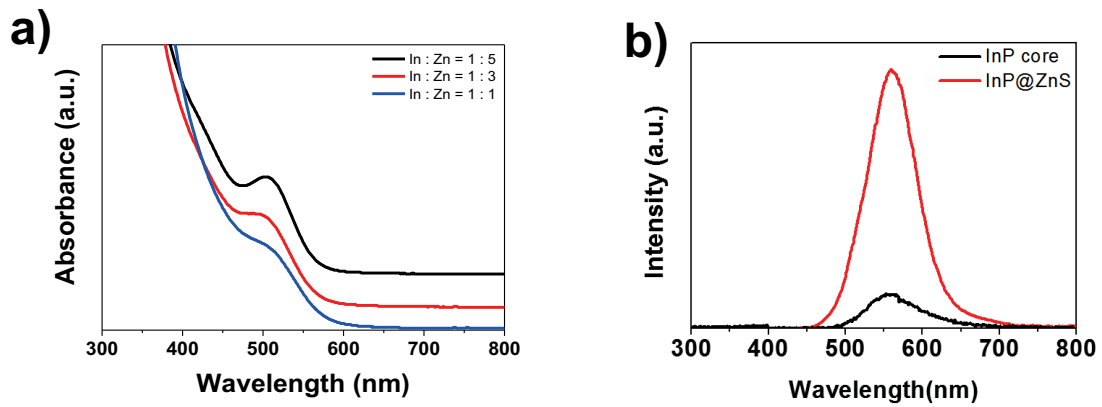
Figure 10. a) UV-Vis absorption spectra of InP QDs synthesized by varying [In/Zn] molar ratios at the reaction time of 30 min at 180 ℃. b) PL spectra of InP and InP@ZnS QDs.
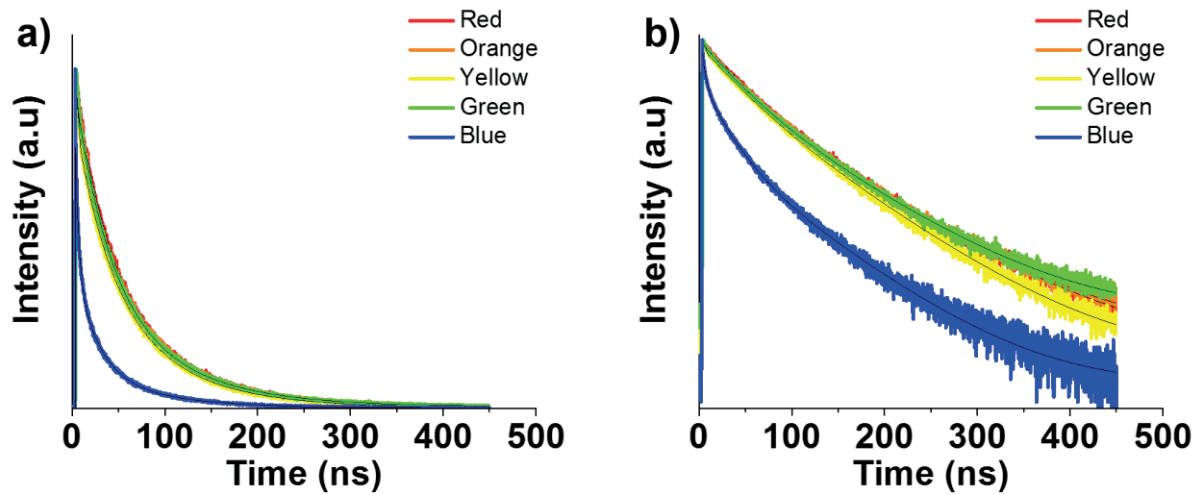
Figure 11. a) Fitting of PL decays (black line) of InP@ZnS QDs with various sizes. PL decays of all types of InP@ZnS QDs were fitted by triexponential model. b) Log scale of PL decays of InP@ZnS QDs.

Table 2. PL decay time components and amplitudes of the triexponential fit curves.

	A_1	τ_1 (ns)	A_2	τ_2 (ns)	A_3	τ_3 (ns)	χ^2	τ_{avg} (ns)
Red	0.26	103.93	0.63	47.40	0.11	10.67	1.15	57.82
Orange	0.26	104.49	0.61	46.95	0.13	9.28	1.33	57.07
Yellow	0.29	95.76	0.61	45.66	0.10	6.54	1.05	55.97
Green	0.23	106.87	0.65	49.75	0.11	12.09	1.16	57.89
Blue	0.16	77.21	0.38	23.48	0.46	3.46	1.28	22.53

2.3.2 Structural Characteristics of InP@ZnS QDs

Structural characteristics of InP@ZnS QDs were investigated with TEM and XRD analyses (Figure 13). TEM images and size histograms of red- and green-emitting InP@ZnS QDs exhibiting PL peaks at 630 and 530 nm, respectively, show monodisperse nanocrystals with the average size of 3.83 ± 0.22 nm for the red-emitting ones and 3.31 ± 0.22 nm for the green-emitting ones (Figure 12a−d). To obtain the size histogram and distribution, the diameter of at least 50 nanocrystals in three or four low-magnification TEM images (Figure 13) was measured. The size of the QDs was estimated based on the assumption that the nanocrystals were spherical. The high-resolution TEM images (depicted in the insets of Figure 12a,b) clearly show lattice fringes of 3.2 Å, indicating the crystalline nature of the QDs. The XRD pattern of InP@ZnS QDs in Figure 12e shows three broad main peaks corresponding to the zinc-blende crystal structure of InP (JCPDS No. 32-0452) with slight peak shifts. These peak shifts are attributed to the lattice contraction arising from an epitaxially grown ZnS shell on the InP core and agree with previously reported observations in the synthesis of InP@ZnS QDs.[70,71]
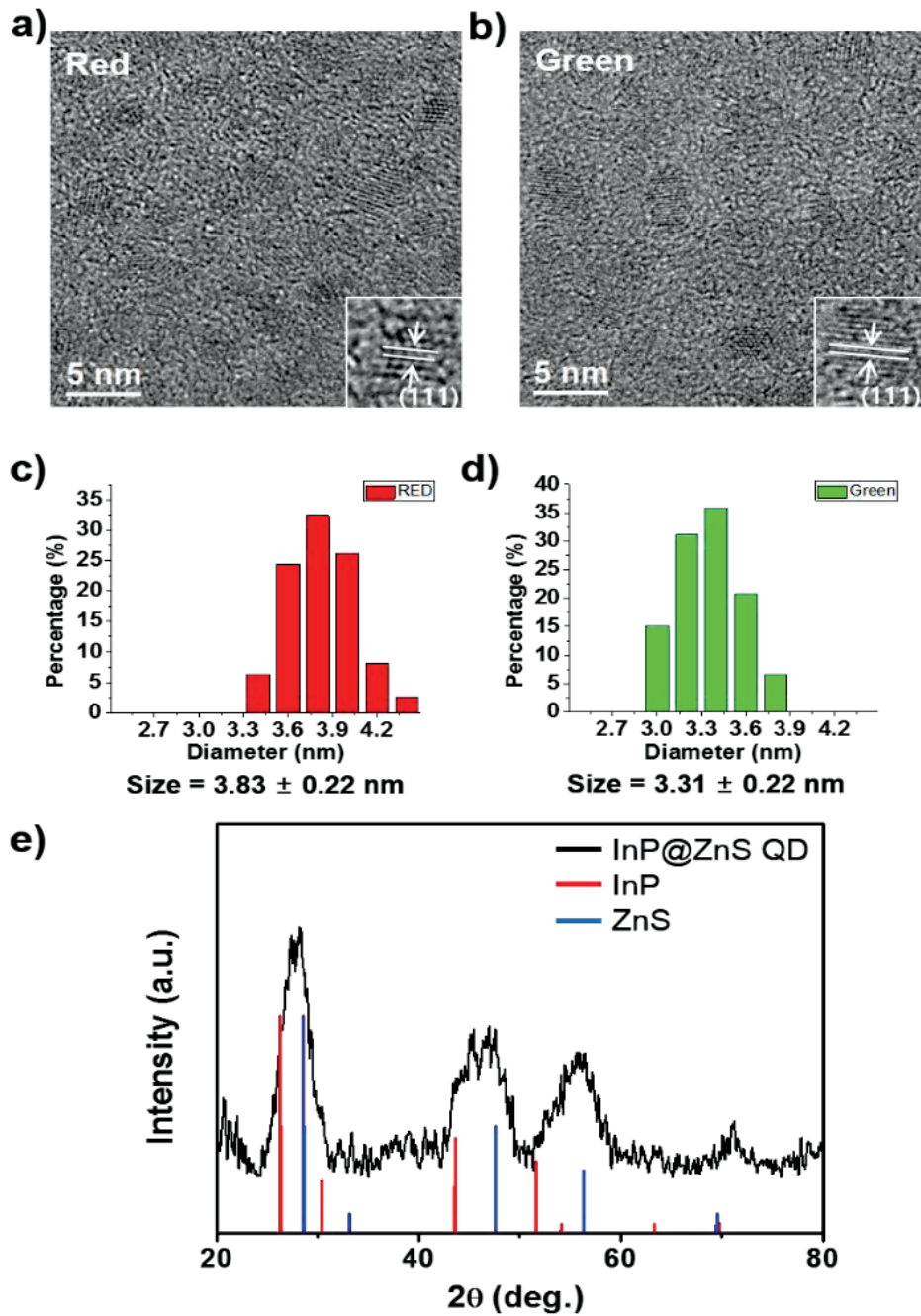
Figure 12. TEM images of a) red- and b) green-emitting InP@ZnS QDs. Size histograms of c) red- and d) green-emitting InP@ZnS QDs. e) XRD pattern of red-emitting InP@ZnS QDs. The vertical lines in a panel e indicate the XRD patterns of bulk InP (blue) and ZnS (red).
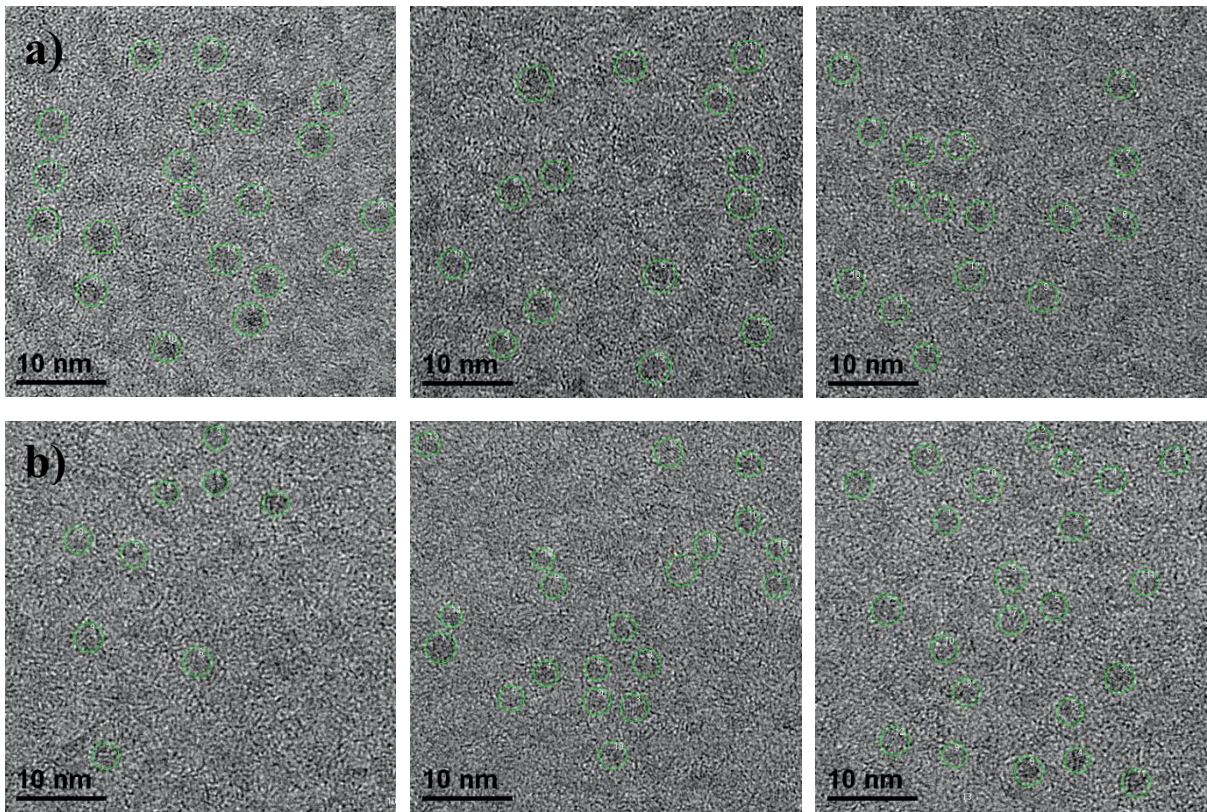
Figure 13. Low-magnification TEM images (500K) of a) green- and b) red –emitting InP@ZnS quantum dots to be used to estimate the size distribution of quantum dots.

2.3.3 Various Reaction Parameters to Control the Size and Size Distribution

In the current synthesis, TOP was found to be the proper solvent to dissolve P_4 and to ensure the monodispersity of the nanocrystals and their high QY, when compared to other high boiling point solvents. For example, I comparatively conducted synthesis experiments of InP QDs with TOP, OLA, and TBP to dissolve P_4 and observed that InP@ZnS QDs synthesized with TOP-P_4 solution showed the sharpest excitonic transition in the absorption spectrum as well as the highest QY in PL spectrum (Figure 14). In addition to the optimization of the P_4 precursor solution, I identified several reaction parameters which are important for the size control and distribution of InP QDs, such as reaction temperatures, growth time, the types and concentration of akylamine, and the type of In precursors. First, the optimized reaction temperature was found to be critical for producing monodispersed InP QDs (Figure 15a). For example, InP QDs synthesized at reaction temperatures higher than 210 °C or lower than 150 °C for 30 min with $InCl_3$ precursor and $ZnCl_2$ additive showed featureless absorption spectra due to their broad size distributions, which indicates an optimum temperature between 150 and 210 °C (Figure 15e,f). Therefore, the green-, yellow-, and orange-emitting QDs were synthesized at reaction temperatures of 150, 180, and 210 °C, respectively.

In addition to the reaction temperature, the accessible size range in a reaction can be controlled by varying the type of indium halide precursors. I performed the synthesis of InP@ZnS QDs where $InCl_3$, $InBr_3$, and InI_3 precursors were used in the presence of $ZnCl_2$ additive under the reaction temperature of 180 °C for 30 min. I found that use of InI_3 in the reaction led to a significant shift of the absorption peak to lower wavelengths. Since halides can be adsorbed on the InP surface, the variation of the binding strength or steric effects may lead to slower growth of QDs (Figure 15b). To verify a halide termination of nanocrystal surfaces, I performed X-ray photoelectron spectroscopy (XPS) analysis on InP QDs synthesized with $InCl_3$ and InI_3 precursor in the presence of $ZnCl_2$. The XPS spectra of InP QDs synthesized with InI_3 (Figure 16a) showed peaks in both, the I 3d and Cl 2p region, whereas peaks only in the Cl 2p region were observed in the spectra of InP QDs synthesized with $InCl_3$ (Figure 16b). This finding demonstrates that the surfaces of InP QDs are passivated with halide ions, which should originate from InX_3 precursors and the $ZnCl_2$ additive. At the same time, I cannot rule out the possibility that the type of InX_3 affects nucleation kinetics because the bond dissociation energy of InX_3 decreases in the order of F^-, Cl^-, Br^-, and I^-.[72] Based on the halide termination effect, I could synthesize the smaller sized and blue-emitting InP@ZnS QDs by using InI_3 precursor and ZnI_2 additive under the same reaction condition for yellow-emitting QDs (Figure 17a).

The size of InP QDs can also be tuned by the amount of alkylamines and their chain length (Figure 15c,d).[73] The syntheses were conducted by using $InCl_3$ precursors and $ZnCl_2$ additive under the reaction temperature of 180 °C for 30 min. To investigate the chain length of alkylamine, 10 mmol of

alkylamine was used for this reaction, regardless of their chain lengths. I found that the size of InP QDs was increased by using alkylamine with shorter chain length. The indium−alkylamine complex formed during the reaction of $InCl_3$ with alkylamine acts as an In source. Thus, the heavier indium−alkylamine complex may diffuse more slowly into the surface layers of growing InP QDs; as a result, smaller QDs are produced.[73] Since OLA (used as a solvent) also acts as a source of surface passivating ligands for QDs, varying its amount may affect the degree of QD surface passivation during the growth stage as well as the size of the resulting QDs. For example, the orange-emitting QDs can be synthesized by using half the amount of OLA, compared with that for yellow-emitting QDs, at 180 °C for 30 min. I also investigated the effect of the precursor ratio between $InCl_3$ and P_4 and observed an increase in size while lowering the In/P ratio (Figure 17b).

Although the various reaction parameters enable adjusting the size of the QDs, the monodispersed red-emitting QDs exhibiting the PL peak at the wavelength higher than 630 nm could not be synthesized under the described conditions. Thus, I performed the experiment that additional P_4 precursor in TOP was injected into the reaction mixture for the synthesis of orange-emitting QDs at 210 °C, making them further grow to form red-emitting QDs exhibiting PL at 630 nm (Figure 18).
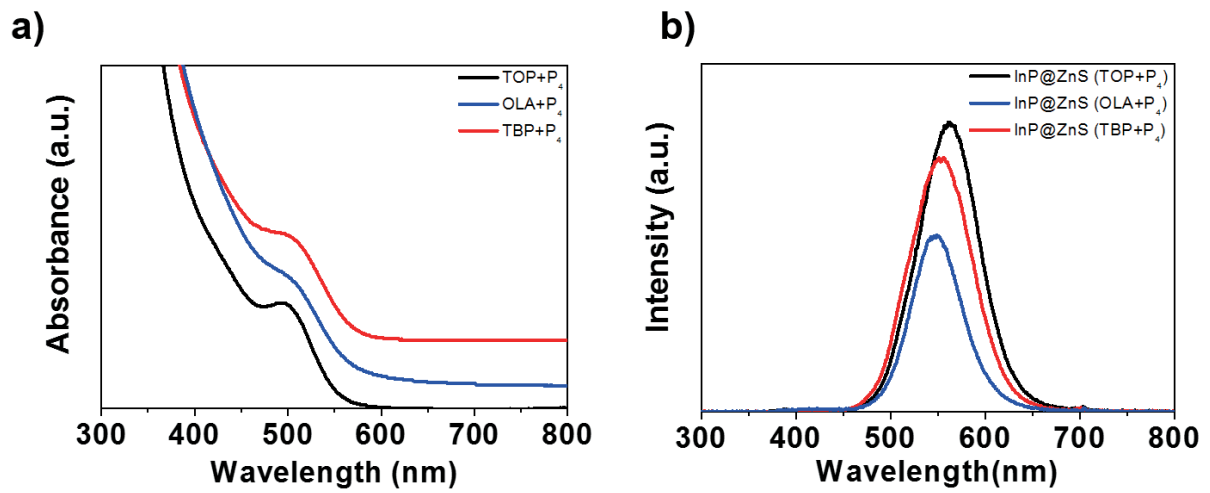
Figure 14. a) Absorption spectra of InP cores b) PL spectra of InP@ZnS QDs using P$_4$ solution in tri-n-butylphosphine (TBP), oleylamine (OLA), and trioctylphosphine (TOP).

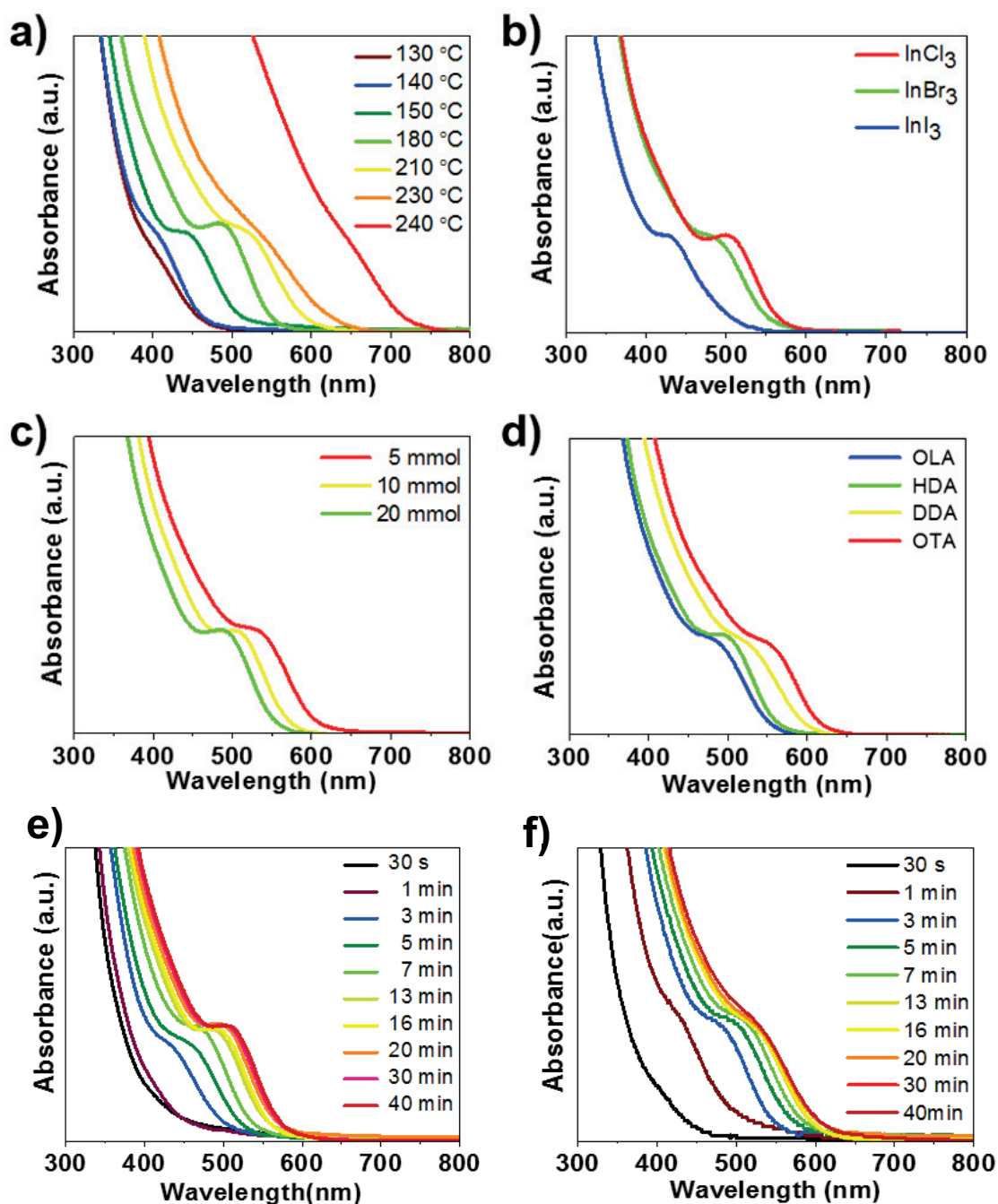**Figure 15.** UV−vis absorption spectra indicating the effect of different reaction parameters on the size evolution of InP nanocrystals: a) temperature; b) indium halide precursor; c) OLA concentration; and d) amine chain length (OLA, HDA, DDA, and OTA indicate oleylamine, hexadecylamine, dodecylamine, and octylamine, respectively). Time-evolution absorption spectra of InP QDs synthesized from e) 180 ℃ and f) 210 ℃.

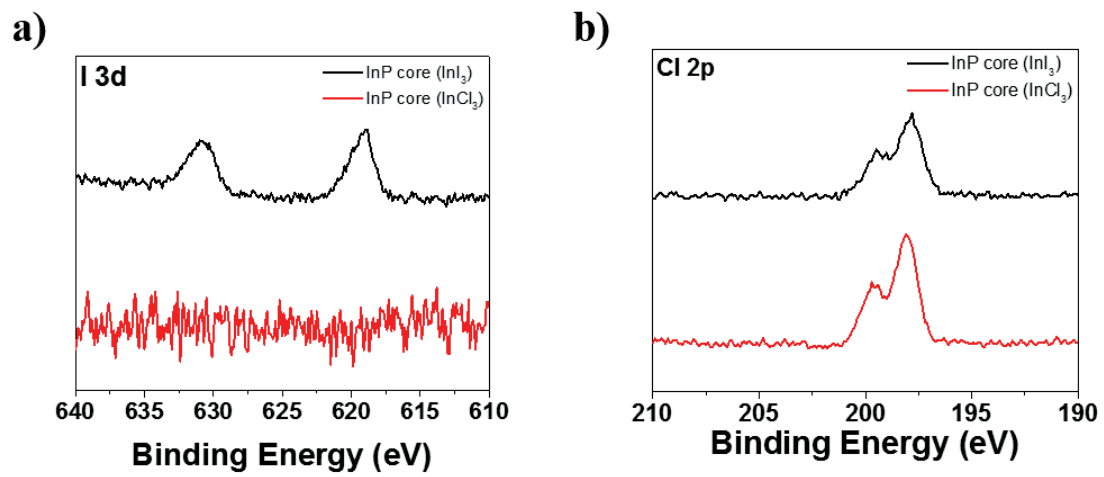**Figure 16.** XPS spectra of InP quantum dots using $InCl_3$ and InI_3 precursors in the a) I 3d range and b) Cl 2p range.
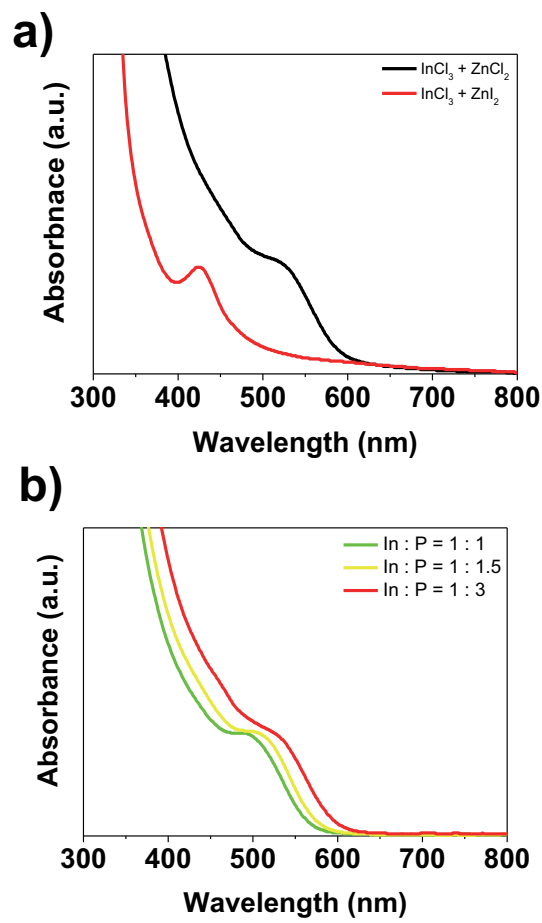
Figure 17. a) UV-Vis absorption spectra of InP@ZnS QDs synthesized with $ZnCl_2$ and ZnI_2 additives. b) of InP core synthesized by varying In/P molar ratios.
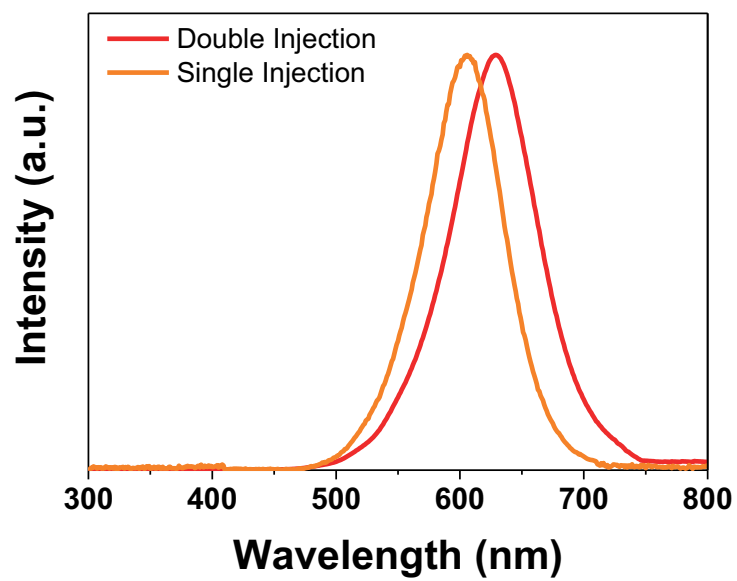
Figure 18. PL spectra of InP@ZnS QDs synthesized by the single and double injections of P_4 precursors.

2.3.4 Reaction Mechanism of InP QDs

Elucidation of possible reaction pathways for the synthesis of InP QDs from P-containing precursors is critical for fabricating highly luminescent QDs because all stages of their formation (such as nucleation, growth, and ripening) are significantly affected by the P precursor reactivity. To investigate the mechanism of the reaction described in this study, the entire process was continuously monitored by ^{31}P NMR spectroscopy. The ^{31}P NMR spectrum of P_4 solution in TOP, OLA, and the mixed solvent of TOP and OLA (Figure 19a) exclusively show peaks corresponding to P_4 and TOP, respectively. Peaks related to red P and any possible reaction products between P_4 and solvents were not detected.[74] This finding demonstrates the high purity of the P_4 precursor for the synthesis of InP QDs. After the injection of the P_4 solution into the In precursor solution, the P_4 peak in the ^{31}P NMR spectrum progressively decreased during the reaction (Figure 19b,c). Furthermore, no other spectral changes were observed during the synthesis except for the decrease in the P_4 peak intensity, indicating that the P_4 precursor reacted directly and only with the In precursor to produce InP without the formation of intermediates (Figure 20a). In addition, no P-containing byproducts were formed during the reaction with P_4. Since no reactive intermediates were obtained from the P_4 precursor in this study, it can be suggested that the P precursor concentration has decreased slowly during the growth of InP QDs, which is further confirmed by the presence of the P_4 peak in the ^{31}P NMR spectrum recorded as late as after 45 min of the reaction.

This result is in sharp contrast to previous studies which reported reaction pathways for the synthesis of InP QDs with various P precursors[58,75-78] because the latter are typically transformed to reactive intermediate species. For example, it has been reported that the widely used P(TMS)$_3$ precursor is transformed to protonated compounds at high temperatures and vigorously reacts with In precursors to form InP QDs.[75,76]

In particular, the recently developed tris(dimethylamino)phosphine(P(NMe$_2$)$_3$) precursor is utilized with indium halides precursors in the presence of a primary alkylamine, of which the reaction conditions are similar to the currently developed methodology using P_4 precursor. In the former synthesis, P(NMe$_2$)$_3$ is fully transformed to P(NHR)$_3$ by the trans-amination reaction with a primary alkylamine used as a solvent. This intermediate product of P(NHR)$_3$ acts as a P precursor to react with In precursors.[77,78] Furthermore, the formation of P(NHR)$_3$ is easily demonstrated by ^{31}P NMR analysis, which clearly shows multiple peaks depending on the number of alkylamines in P(NHR)$_x$ in the range of 0−120 ppm. However, in the current synthesis, I could not observe any peaks related to the formation of P(NHR)$_3$. The enlarged ^{31}P NMR spectra in the range of 0−120 ppm showed solely the peaks related to TOP (Figure 20b). Although the current synthesis shares the similarity with that using P(NMe$_2$)$_3$ precursor, these results demonstrate the different reaction mechanisms for the

formation of InP QDs.

Considering the oxidation states of the In precursor (In^{3+}), three electrons should be supplied to the reaction to form the InP structure. In the current reaction, to specifically identify the reducing agent, I conducted control experiments in which OLA or TOP were replaced with an inert solvent, in detail 1-octadecene (ODE). In this case, I found that the reaction did not occur in the absence of OLA (Figure 21a). This observation hints at the reducing effect of OLA on the reaction between In and P precursors. The previous reports on the synthesis of InP QDs using indium halides also suggested the importance of the reducing effect for forming InP structures. Xie et al. reported the solvothermal synthesis of InP nanocrystals using $InCl_3$ in the presence of the reducing agent KBH_4.[56] Similarly, in two recent mechanistic studies of InP QDs by Tessier et al.[77] and by Mézailles et al.,[78] the authors pointed out the additional role of tris(diethylamino)-phosphine $P(NEt_2)_3$) precursor as reducing agent in its reaction with indium halides.

TOP is often utilized as a P source for the synthesis of metal phosphide nanocrystals.[79,80] It is difficult to rule out the possibility that TOP acts as a P source in our synthesis rather than a solvent. To clarify this issue, I performed a control experiment where only TOP was injected into the reaction mixture instead of TOP-P_4 solution. As shown in Figure 21b, the reaction mixture with TOP injection does not exhibit any absorption characteristics in the visible range. This finding demonstrates that TOP did not act as a P source in our synthesis of InP QDs.

Figure 19. a) 31P NMR spectra of solutions of P4 in TOP, OLA, and the mixed solvent of TOP and OLA. b) 31P NMR spectra of the aliquots taken from the reaction mixture during the synthesis. c) Concentration profiles of P4 during the synthesis of InP.

a)

b)

Figure 20. a) Full-scale time-resolved ^{31}P-NMR spectra of the reaction solutions for the synthesis of InP QDs. b) The enlarged 31P-NMR spectra of TOP and solutions of P$_4$ in TOP, the mixed solvent of TOP and OLA.

Figure 21. a) Absorbance spectra of InP QDs with different type of solvents. b) Absorption spectrum of the product obtained with TOP as a P precursor and TOP+P_4 precursor.

2.3.5 Large-scale synthesis of InP@ZnS QDs

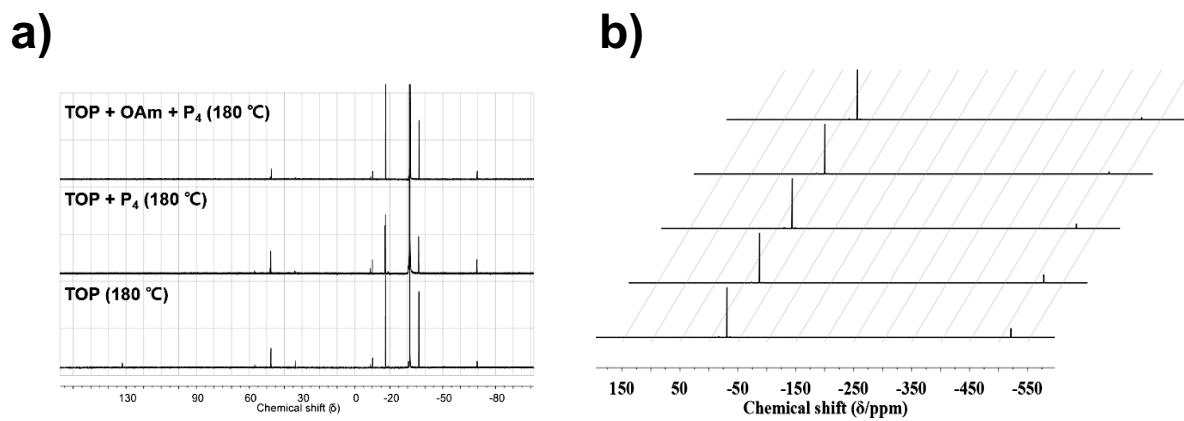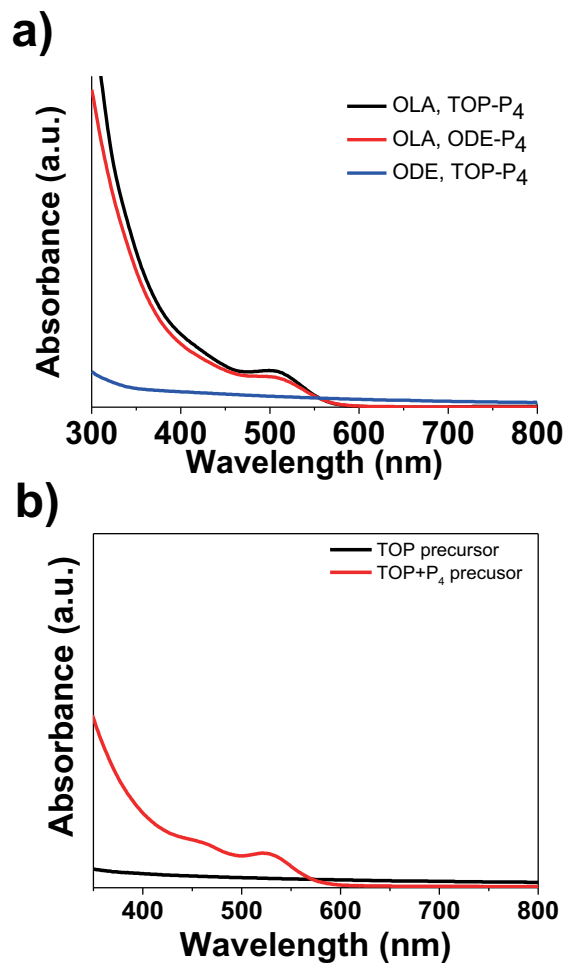The described characteristics of the P_4 precursor, including its relatively slow reaction with indium halides, can offer the possibility of large-scale production of high-quality InP QDs. In fact, by today typically used P precursor P(TMS)$_3$ has a critical issue of fast depletion at high temperatures. This limitation restricts the production of InP QDs in a large-scale batch to a reaction which is less sensitive to the homogeneity of the reaction mixture. As an alternative, the relatively slow reaction of P_4-TOP can provide a solution to this challenge. Thus, scaling up the batch reaction for InP QDs by a factor of 10 successfully yielded 6.3 g of InP@ZnS QDs (Figure 22a). Furthermore, the synthesized QDs exhibited a QY of 51% in the PL spectrum with a fwhm of 70 nm, which is comparable to the values obtained for the QDs from the small-scale synthesis (Figure 22b). These results highlight the applicability of the proposed synthetic method to produce high-quality emitters on a large scale.
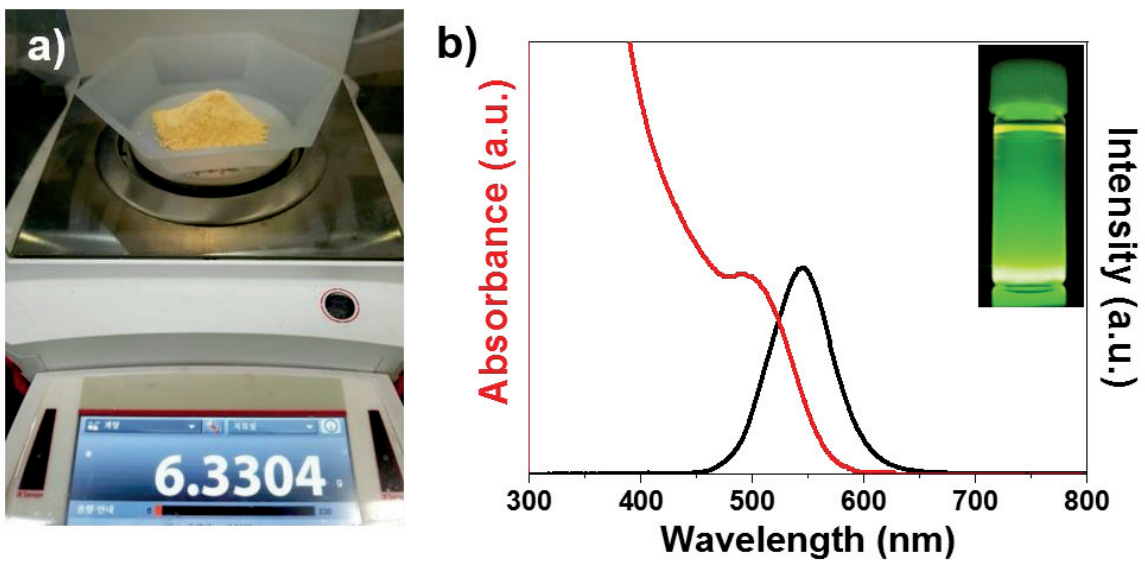
Figure 22. (a) Photograph showing the amount of final product QDs obtained by a single-batch reaction. (b) UV−vis and PL spectra of corresponding InP@ZnS QDs. The inset shows the photograph of corresponding InP@ZnS QDs solution under UV irradiation.

2.4 Conclusion

In summary, I developed a new type P precursor based on P_4 for the synthesis of highly luminescent InP@ZnS QDs. This precursor was easily synthesized from red P powder, which is the cheapest form of P existing on Earth's crust. I systematically studied various reaction parameters to control the size and size distribution of InP@ZnS QDs and therefore, tuning the luminescence color across the entire visible range with the high QY of InP@ZnS QDs (over 60%). In addition, the reaction pathway for the current synthesis using P_4 precursor was investigated by monitoring the reaction during the growth of InP QDs using ^{31}P NMR analysis and I found that P_4 precursor directly and slowly reacted with In precursor without the formation of reactive intermediate species. Thus, the relatively low reactivity of P_4 precursor could allow for the large-scale production of InP@ZnS QDs, yielding more than 6 g of QDs per one-batch reaction. The proposed new type of P precursor can be widely utilized in various fields of chemistry. Moreover, I strongly believe that the currently developed approach will pave the way to produce high-quality economic QD emitters, shedding new light on the QD display industry.

Chapter III. Synthesis of InP colloidal quantum dots with combined phosphorus sources.

3.1 Introduction

InP has emerged as a new light emitting material to replace CdSe, but has a problem that its luminescence characteristics are weaker than those of Group 2-6. In addition, the relatively broad size distribution of InP makes the segregation of nucleation and growth stages more difficult. The first is due to the more covalent nature of the ionic properties of groups 2-6, and the second is due to the rapid depletion of molecular precursors at higher temperatures. Especially, the reason of this rapid depletion is due to TMSP, which is a P precursor which is mainly used for InP synthesis. The TMSP precursor in the allen group was found to deplete very rapidly without leaving any molecular phosphorus precursors capable of monomer formation during the growth step at high temperatures. This prevents the supply of phosphorus monomers necessary for growth after the InP quantum dot nucleation reaction. When Phosphorus is stopped, quantum dots cannot be grown by monomer, but by Oswald ripening by non-molecular InP species. These growth steps through Ostwald ripening are associated with increased polydispersity. For this reason, the size distribution is poor compared to the II-VI material.

In order to solve these problems, I use p precursors with different reaction rates. I have attempted to synthesize homogeneous and stable InP nanoparticles by separating the growth using a relatively fast P precursor using the nucleation step and a slow P precursor. White phosphorus was used for the slow P precursor and TMSP and DEAP for the fast P precursor. Especially, DEAP synthesis method uses precursors similar to white phosphorus, but its mechanism is very different. In the case of DEAP, InP occurs as a transamination reaction, but in the case of WP, P directly reacts. Therefore, I can easily synthesize InP quantum dots of homogeneous particles by separating the P precursor acting on the nucleation and the P precursor acting on the growth without further injection by using the difference in reactivity.

3.2 Experimental session

3.2.1 Materials

Indium(III) chloride (99.999%), zinc(II) chloride (98+ %), oleylamine (OLA, 98+%), tri-n-octylphosphine (TOP, 97%), trisdiethylaminophosphine(DEAP,98%) were purchased from Sigma-Aldrich. Phosphorus powder (98.9%) was purchased from Alfa Aesar. All chemicals above were used directly without any purification.

3.2.2 Synthesis of InP core using combined phosphorus

A 0.3 mmol of indium chloride and 1.47 mmol of zinc chloride were dissolved in 1.64 mL of OLA in a 50 mL three-neck flask. This solution was degassed at 120 °C for 1 h and then heated to 180 °C under inert atmosphere. A 37mg amount of P_4 powder was dissolved into TOP at 80 °C for several minutes. After cooling to room temperature, add 0.1 mmol of TMSP or DEAP. Subsequently, the solution was injected into the reaction mixture in the batch, which was kept at that temperature for 30 min.

3.3 Result and Discussion

I compared amino phosphorus and white phosphorus about combined phosphorus. As the ratio of P to Indium increases, the amino phosphorus shifts to blue while the white phosphorus shift to red.(figure 17 b and figure 23 a) When the amount of OLA is varied, it also shows a different tendency.(figure 15 c and figure 23 b) When the amount of the OLA increases for synthesis using the white phosphorus precursor blue shift, however, for the synthesis using the DEAP show the opposite trend. This means that the entering precursors are similar, but have different mechanisms. In this way, I tried to achieve uniform synthesis by separating nucleation and growth through combine with other phosphorus. First, WP is injected to form a monomer, and DEAP or TMSP, which is relatively rapidly generated, is injected to form nucleation.
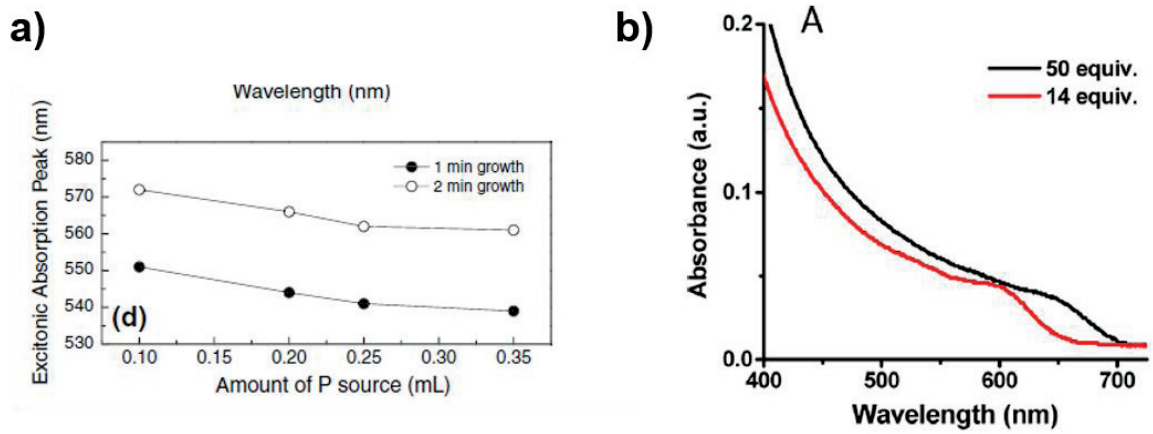
Figure 23. Absorption peak change according to a) In / P ratio and b) OLA of InP synthesized with DEAP.

3.3.1. TMSP + WP combined phosphorus

I experimented with mixing TMSP and WP. TMSP, as mentioned in the Intro, is the most commonly used P precursor and has the fastest reactivity. Using a ratio of TMSP to WP of 0.1: 1, nucleation is caused by the addition of a very small amount of TMSP. The remaining amount was formed as a monomer together with a large amount of WP to induce the growth process. Usually, the reaction temperature of TMSP is 300 °C. In this context, as shown in figure 24 a, the uv-vis confirms that no dot is formed at temperatures below 300 °C. In case of the peak at 180 °, cluster appears as the region appearing in the cluster. At 250 ° C, the red shift was more reversible than the 180 ° C but the first excitonic peak was not found. The formation of the dot at 300 ° C was confirmed by the TEM image. Figure 24 b is TEM data of InP synthesized with WP and TMSP at 300 ° C, and the dot size of about 4 nm was confirmed. Figure 24 c is the uv-vis data which reacted at 300 °C with just TMSP and TMSP WP together. When not at all, first excitonic peak was observed at around 450 nm, but when it was put together, red shift occurred at around 630 nm. This is the result of showing that the insertion of WP helps the growth of nucleation formed by TMSP. I also found that the XRD data is well matched to InP. (figure 24 d) TMSP has a disadvantage that it is difficult to reach the red region, but it shows the possibility of InP synthesis in the NIR region by using it with WP.

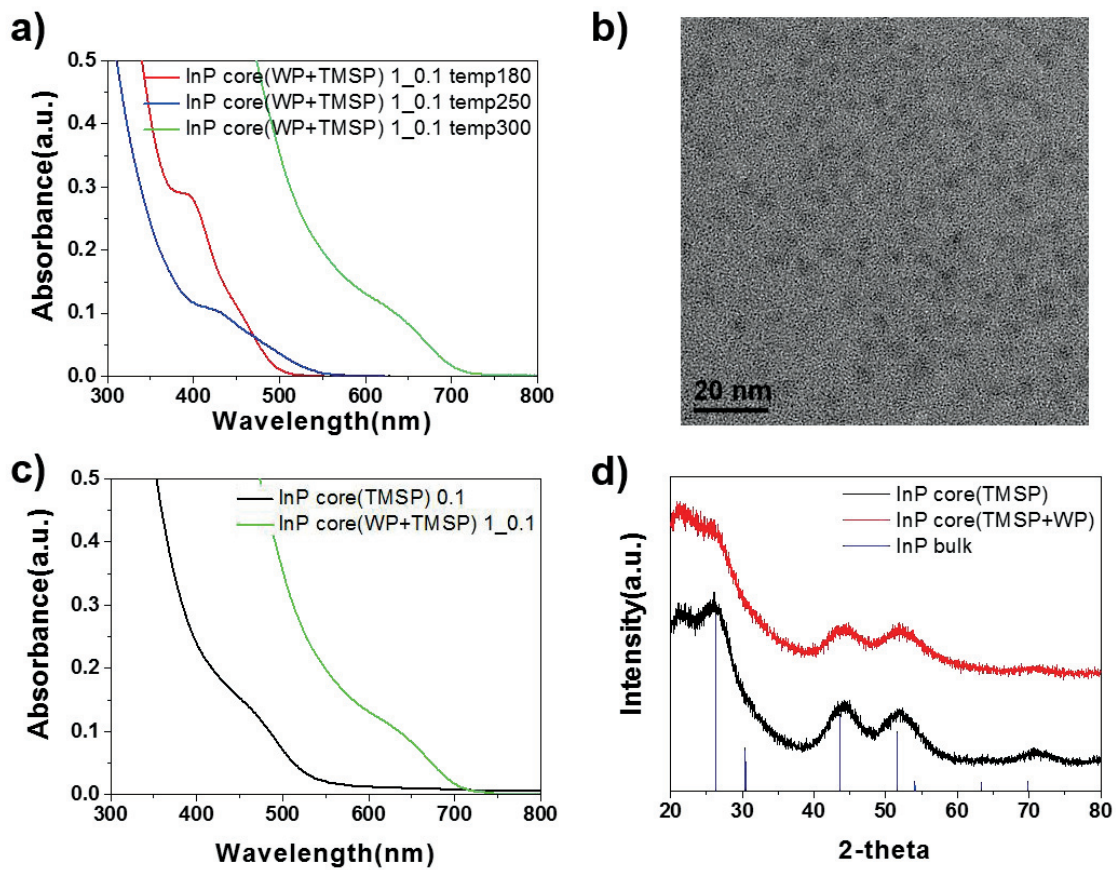**Figure 24.** (a) Absorbance change according to the temperature of the InP core with $(TMS)_3P$ and P_4. (b) TEM of InP core synthesized using $(TMS)_3P$ and P_4 at 300 °C. (c) Absorbance change in the presence of P_4. (d) XRD data of InP core with only $(TMS)_3P$ and $(TMS)_3P + P_4$ combined phosphorus.

3.3.2. DEAP + WP combined phosphorus

We used DEAP and WP together to synthesize InP core. First, since the tendency between two precursors is different, it is judged that the mechanism is different, and the experiment on the ratio is performed first. Figure 25a shows the uv-vis data that attempted to adjust the amount of nucleation by fixing the amount of WP and changing the amount of DEAP. According to the previous assumption, as the amount of DEAP increases, the number of nucleation increases, so the result of blue shifting of uv-vis data should be shown. However, in the case of experiment with WP, the first excitonic peak showed little difference even though the amount of DEAP was increased, so that it can be seen that the number of nucleation does not greatly differ even if the amount increases. However, blue shifted compared to the InP core containing only DEAP. This was also the opposite of the assumption that WPs grow as monomers that help growth. (Figure 25b) This time, the amount of DEAP was fixed and the amount of WP was increased. When the amount of WP was increased, (Figure 25c). In order to reveal this, we considered that the TOP was mixed with the WP, fixed the amount of DEAP and injected TOP only. As shown in figure 25d, blue shift was observed as the amount of TOP increased, and the distribution of TOP increased as the amount of TOP increased. It seems that the overall concentration affected TOP.
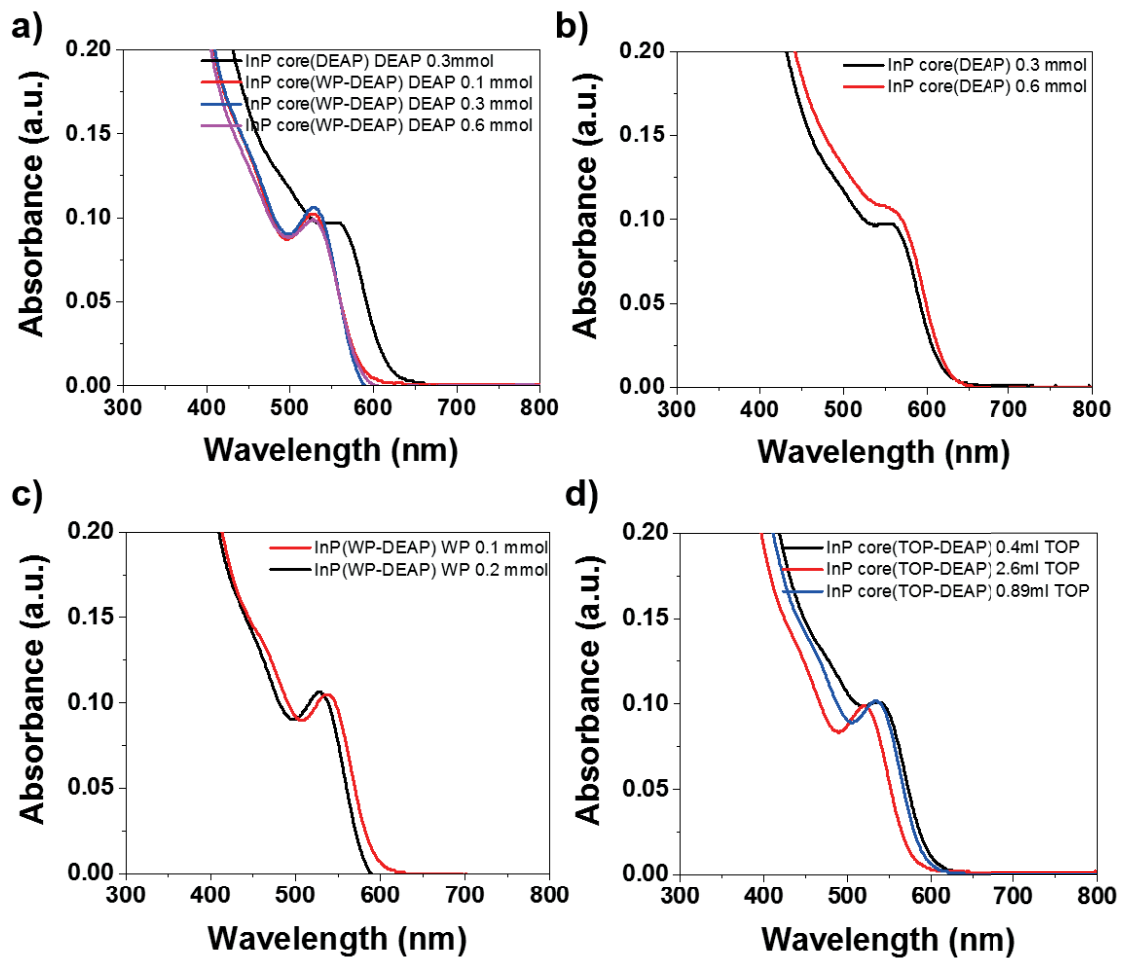
Figure 25. Absorbance change (a) in the amount DEAP with WP(P$_4$), (b) in the amount DEAP only, (c) in the amount WP(P$_4$), (d) in the amount TOP with DEAP.

3.4 Conclusion

I tried to synthesize uniform nanoparticle following Lamer model. The combination of TMSP and WP, DEAP and WP was tried by mixing precursor. In the case of InP core using TMSP and WP, TEM image shows that the dot is synthesized at over 300 degrees. In addition, as the assumption was made, the size was increased through the uv-vis data rather than the InP core using only TMSP. Also, when TMSP was used together, it was also found that the crystallinity was increased by XRD data. When InP core was synthesized by mixing DEAP and WP, it was blue shifted when the amount of WP was fixed and the amount of DEAP was changed. This was due to the influence of TOP, which is a solvent used with solid WP, that blue shift and size distribution were better as the amount of TOP was increased. Using two P precursors together, we solved the problem of using only TMSP and confirmed that the size distribution was also improved. This suggests the possibility of more uniform and variable size InP QD synthesis.

Conclusion

In summary, I developed a new type P precursor based on P_4 for the synthesis of highly luminescent InP@ZnS QDs. This precursor was easily synthesized from red P powder, which is the cheapest form of P existing on Earth's crust. I systematically studied various reaction parameters to control the size and size distribution of InP@ZnS QDs and therefore, tuning the luminescence color across the entire visible range with the high QY of InP@ZnS QDs (over 60%). In addition, the reaction pathway for the current synthesis using P_4 precursor was investigated by monitoring the reaction during the growth of InP QDs using ^{31}P NMR analysis and I found that P_4 precursor directly and slowly reacted with In precursor without the formation of reactive intermediate species. Thus, the relatively low reactivity of P_4 precursor could allow for the large-scale production of InP@ZnS QDs, yielding more than 6 g of QDs per one-batch reaction.

Also, I tried to synthesize uniform nanoparticle following Lamer model. The combination of TMSP and WP, DEAP and WP was tried by mixing precursor. In the case of InP core using TMSP and WP, TEM image shows that the dot is synthesized at over 300 degrees. In addition, as the assumption was made, the size was increased through the uv-vis data rather than the InP core using only TMSP. Also, when TMSP was used together, it was also found that the crystallinity was increased by XRD data. When InP core was synthesized by mixing DEAP and WP, it was blue shifted when the amount of WP was fixed and the amount of DEAP was changed. This was due to the influence of TOP, which is a solvent used with solid WP, that blue shift and size distribution were better as the amount of TOP was increased. Using two P precursors together, we solved the problem of using only TMSP and confirmed that the size distribution was also improved. This suggests the possibility of more uniform and variable size InP QD synthesis.

The proposed new type of P precursor can be widely utilized in various fields of chemistry. Moreover, I strongly believe that the currently developed approach will pave the way to produce high-quality economic QD emitters, shedding new light on the QD display industry.

References

1. Jeremy norman's history, 2017, "Discovery of Quantum Dots", http://www.historyofinformation.com/expanded.php?id=3886.

2. Efros, AI. L.; Efros, A. L. Interband Absorption of Light in a Semiconductor Sphere. *Sov. Phys. Semicond.* **1982**, *16*, 772−775.

3. H. S. Nalwa, *Handbook of Nanostructured Materials and Nanotechnology*, Academic Press, New York, 2000.

4. Zrazhevskiy, P.; Sena, M.; Gao,X. Designing multifunctional quantum dots for bioimaging, detection, and drug delivery. *Chem. Soc. Rev.*, **2010**, *39*, 4326.

5. Donega, C. M. Synthesis and properties of colloidal heteronanocrystals, *Chem. Soc. Rev.*, **2011**, *40*, 1512–1546

6. Reiss, P.; Protiere, M.; Li, L. Core/shell Semiconductor Nanocrystals. *Small.* **2009**, *5*, 154.

7. Hines, M. A.; Guyot-Sionnest, P. Synthesis and Characterization of Strongly Luminescing ZnS-Capped CdSe Nanocrystals. *J. Phys. Chem.* **1996**, *100*, 468.

8. Talapin, D. V.; Mekis, I.; Götzinger, S.; Kornowski, A.; Benson, O.; Weller, H. CdSe/CdS/ZnS and CdSe/ZnSe/ZnS Core-Shell-Shell Nanocrystals. J. Phys. Chem. B. 2004, 108, 18826.

9. Xu, S.; Ziegler, J.; Nann, T. Rapid Synthesis of Highly Luminescent InP and InP/ZnS Nanocrystals. *J. Mat. Chem.* **2008**, *18*, 2653.

10. Colvin, V.; Schlamp, M.; Alivisatos, A. P. Light-emitting-diodes made from cadmium selenide nanocrystals and a semiconducting polymer. *Nature* **1994**, *370*, 354−357.

11. Coe, S.; Woo, W.-K.; Bawendi, M.; Bulović, V. Electroluminescence from single monolayers of nanocrystals in molecular organic devices. *Nature* **2002**, *420*, 800−803.

12. Huynh, W. U.; Peng, X.; Alivisatos, A. P. CdSe nanocrystal rods/poly(3-hexylthiophene) composite photovoltaic devices. *Adv. Mater.* **1999**, *11*, 923.

13. Huynh, W. U.; Dittmer, J. J.; Alivisatos, A. P. Hybrid nanorodpolymer solar cells. *Science* **2002**, *295*, 2425−2427.

14. Gur, I.; Fromer, N. A.; Geier, M. L.; Alivisatos, A. P. Air-stable allinorganic nanocrystal solar cells processed from solution. *Science* **2005**, *310*, 462−465.

15. Bruchez, M.; Moronne, M.; Gin, P.; Weiss, S.; Alivisatos, A. P. Semiconductor nanocrystals as fluorescent biological labels. *Science* **1998**, *281*, 2013−2016.

16. Zakharov, O.; Rubio, A.; Blase, X.; Cohen, M. L.; Louie, S. G. Quasiparticle band structures of six II-VI compounds: ZnS, ZnSe, ZnTe, CdS, CdSe, and CdTe. *Physical Review B*, **1994**, *50*, 10780.

17. Tamang, S.; Lincheneau, C.; Hermans, Y.; Jeong, S.; Reiss, P. Chemistry of InP Nanocrystal

Syntheses, *Chem. Mater.* **2016**, *28*, 2491−2506.

18. Murray, C. B.; Norris, D. J.; Bawendi, M. G. Synthesis and Characterization of Nearly Monodisperse CdE(E = sulfur, selenium, tellurium) Semiconductor Nanocrystals. *J. Am. Chem. Soc.* **1993**, *115*, 8706−8715.

19. Peng, Z. A.; Peng, X. Formation of high-quality CdTe, CdSe, and CdS nanocrystals using CdO as precursor. *J. Am. Chem. Soc*, **2001**, *123*, 183-184.

20. Kadlag, K. P.; Patil, P.; Jagadeeswara Rao, M.; Datta, S.; Nag, A. Luminescence and Solar Cell from Ligand-Free Colloidal AgInS$_2$ Nanocrystals. *CrystEngComm*. **2014**, *16*, 605−3612.

21. Li, L.; Daou, T. J.; Texier, I.; Kim Chi, T. T.; Liem, N. Q.; Reiss, P. Highly luminescent CuInS$_2$/ZnS core/shell nanocrystals: cadmium-free quantum dots for in vivo imaging. *Chem. Mater.*, **2009**, *21*, 2422-2429.

22. Renguo, X.; Battaglia, D.; Peng, X. Colloidal InP nanocrystals as efficient emitters covering blue to near-infrared. *Journal of the American Chemical Society*, **2007**, *129*, 15432-15433.

23. Green, M.; O'Brien, P. A novel metalorganic route for the direct and rapid synthesis of monodispersed quantum dots of indium phosphide. *Chem. Commun.* **1998**, 2459−2460.

24. Jun, K.-W.; Khanna, P. K.; Hong, K.-B.; Baeg, J.-O.; Suh, Y.-D. Synthesis of InP nanocrystals from indium chloride and sodium phosphide by solution route. *Mater. Chem. Phys.* **2006**, *96*, 494−497.

25. Li, L.; Protierè, M.; Reiss, P. Economic Synthesis of High Quality InP Nanocrystals Using Calcium Phosphide as the Phosphorus Precursor. *Chem. Mater.* **2008**, *20*, 2621−2623.

26. Liu, Z.; Kumbhar, A.; Xu, D.; Zhang, J.; Sun, Z.; Fang, J. Coreduction Colloidal Synthesis of III−V Nanocrystals: The Case of InP. *Angew. Chem.* **2008**, *120*, 3596−3598.

27. Bang, E; Choi, Y; Suh, Y. H.; Ban, H. W.; Son. J. S.; Park, J. Large-scale Synthesis of Highly Luminescent InP@ZnS Quantum Dots Using Elemental Phosphorus Precursor. *Chem. Mater.* **2017**, *29*, 4236-4243.

28. Ekimov, A. I.; Efros, A. L.; Onushchenko, A. A. Quantum Size effect in semiconductor microcrystals. *Solid State Commun.* **1985**, *56*, 921−924.

29. Tolbert, S. H.; Alivisatos, A. P. Size Dependence of The Solid-Solid Phase Transition in CdSe Nanocrystals. *Z. Phys. D: At., Mol. Clusters* **1993**, *26*, 56−58.

30. Dabbousi, B. O.; Rodriguez-Viejo, J.; Mikulec, F. V.; Heine, J. R.; Mattoussi, H.; Ober, R.; Jensen, K. F.; Bawendi, M. G. (CdSe)ZnS Core-Shell Quantum Dots: Synthesis and Characterization of a Size Series of Highly Luminescent Nanocrystallites. *J. Phys. Chem. B.* **1997**, *101*, 9463−9475.

31. Talapin, D. V.; Lee, J.-S.; Kovalenko, M. V.; Shevchenko, E. V. Prospects of Colloidal Nanocrystals for Electronic and Optoelectronic Applications. *Chem. Rev.* **2010**, *110*,

389−458.

32. Tang, J.; Sargent, E. H. Infrared Colloidal Quantum Dots for Photovoltaics: Fundamentals and Recent Progress. *Adv. Mater.* **2011**, *23*, 12−29.

33. Zhitomirsky, D.; Furukawa, M.; Tang, J.; Stadler, P.; Hoogland, S.; Voznyy, O.; Liu, H.; Sargent, E. H. N-type Colloidal-Quantum-Dot Solids for Photovoltaics. *Adv. Mater.* **2012**, *24*, 6181−6185.

34. Swarnkar, A.; Shanker, G. S.; Nag, A. Organic-Free Colloidal Semiconductor Nanocrystals as Luminescent Sensors for Metal Ions and Nitroaromatic Explosives. *Chem. Commun.* **2014**, *50*, 4743−4746.

35. Colvin, V. L.; Schlamp, M. C.; Alivisatos, A. P. Light-Emitting-Diodes Made from Cadmium Selenide Nanocrystals and a Semiconducting Polymer. *Nature* **1994**, *370*, 354−357.

36. Coe, S.; Woo, W. K.; Bawendi, M. G.; Bulović, V. Electroluminescence from Single Monolayers of Nanocrystals in Molecular Organic Devices. *Nature* **2002**, *420*, 800−803.

37. Tessler, N.; Medvedev, V.; Kazes, M.; Kan, S.-H.; Banin, U. Efficient Near-Infrared Polymer Nanocrystal Light-Emitting-Diodes. *Science* **2002**, *295*, 1506−1508.

38. Popović, Z.; Liu, W.; Chauhan, V. P.; Lee, J.; Wong, C.; Greytak, A. B.; Insin, N.; Nocera, D. G.; Fukumura, D.; Jain, R. K.; Bawendi, M. G. A Nanoparticle Size Series for In Vivo Fluorescence Imaging. *Angew. Chem.* **2010**, *122*, 8831−8834.

39. Dubertret, B.; Skourides, P.; Norris, D. J.; Noireaux, V.; Brivanlou, A. H.; Libchaber, A. In Vivo Imaging of Quantum Dots Encapsulated in Phospholipid Micelles. *Science* **2002**, *298*, 1759−1762.

40. Kim, S.; Lim, Y. T.; Soltesz, E. G.; De Grand, A. M.; Lee, J.; Nakayama, A.; Parker, J. A.; Mihaljevic, T.; Laurence, R. G.; Dor, D. M.; Cohn, L. H.; Bawendi, M. G.; Frangioni, J. V. Near-Infrared Fluorescent Type II Quantum Dots for Sentinel Lymph Node Mapping. *Nat. Biotechnol.* **2004**, *22*, 93−97.

41. Medintz, I. L.; Uyeda, H. T.; Goldman, E. R.; Mattoussi, H. Quantum Dot Bioconjugates For Imaging, Labelling and Sensing. *Nat. Mater.* **2005**, *4*, 435−446.

42. Sun, Q.; Wang, Y. A.; Li, L. S.; Wang, D.; Zhu, T.; Xu, J.; Yang, C.; Li, Y. Bright, Multicoloured Light-Emitting Diodes Based on Quantum Dots. *Nat. Photonics* **2007**, *1*, 717−722.

43. Zhao, J.; Bardecker, J. A.; Munro, A. M.; Liu, M. S.; Niu, Y.; Ding, I. K.; Luo, J.; Chen, B.; Jen, A. K. Y.; Ginger, D. S. Efficient CdSe/CdS Quantum Dot Light-Emitting Diodes Using a Thermally Polymerized Hole Transport Layer. *Nano Lett.* **2006**, *6*, 463−467.

44. Steckel, J. S.; Snee, P.; Coe-Sullivan, S.; Zimmer, J. P.; Halpert, J. E.; Anikeeva, P.; Kim, L.

A.; Bulovic, V.; Bawendi, M. G. Color-Saturated Green-Emitting QD-LEDs. *Angew. Chem., Int. Ed.* **2006**, *45*, 5796−5799.

45. Lim, J.; Jeong, B. G.; Park, M.; Kim, J. K.; Pietryga, J. M.; Park, Y. S.; Klimov, V. I.; Lee, C.; Lee, D. C.; Bae, W. K. Influence of Shell Thickness on the Performance of Light-Emitting Devices Based on CdSe/Zn1‑xCdxS Core/Shell Heterostructured Quantum Dots. *Adv. Mater.* **2014**, *26*, 8034−8040.

46. Ramasamy, P.; Kim, B.; Lee, M. S.; Lee, J. S. Beneficial Effects of Water in The Colloidal Synthesis of InP/ZnS Core−Shell Quantum Dots for Optoelectronic Applications. *Nanoscale* **2016**, *8*, 17159−17168.

47. Kim, S.; Kim, T.; Kang, M.; Kwak, S. K.; Yoo, T. W.; Park, L. S.; Yang, I.; Hwang, S.; Lee, J. E.; Kim, S. K.; Kim, S.-W. Highly Luminescent InP/GaP/ZnS Nanocrystals and Their Application to White Light-Emitting Diodes. *J. Am. Chem. Soc.* **2012**, *134*, 3804−3809.

48. Yang, X.; Zhao, D.; Leck, K. S.; Tan, S. T.; Tang, Y. X.; Zhao, J.; Demir, H. V.; Sun, X. W. Full Visible Range Covering InP/ZnS Nanocrystals with High Photometric Performance and Their Application to White Quantum Dot Light-Emitting Diodes. *Adv. Mater.* **2012**, *24*, 4180−4185.

49. Franke, D.; Harris, D. K.; Xie, L.; Jensen, K. F.; Bawendi, M. G. The Unexpected Influence of Precursor Conversion Rate in the Synthesis of III-V Quantum Dots. *Angew. Chem., Int. Ed.* **2015**, *54*, 14299−14303.

50. Joung, S.; Yoon, S.; Han, C.-S.; Kim, Y.; Jeong, S. Facile synthesis of uniform large-sized InP nanocrystal quantum dots using tris (tert-butyldimethylsilyl) phosphine Nanoscale. *Nanoscale Res. Lett.* **2012**, *7*, 93.

51. Gary, D. C.; Glassy, B. A.; Cossairt, B. M. Investigation of Indium Phosphide Quantum Dot Nucleation and Growth Utilizing Triarylsilylphosphine Precursors. *Chem. Mater.* **2014**, *26*, 1734−1744.

52. Wells, R. L.; Pitt, C. G.; McPhail, A. T.; Purdy, A. P.; Shafieezad, S.; Hallock, R. B. The use of tris(trimethylsilyl)arsine to prepare gallium arsenide and indium arsenide. *Chem. Mater.* **1989**, *1*, 4−6.

53. Luo, Y.-R. Comprehensive Handbook of Chemical Bond Energies; CRC Press: Boca Raton, FL, USA, 2007.

54. Healy, M. D.; Laibinis, P. E.; Stupik, P. D.; Barron, A. R. The reaction of indium(III)chloride with tris(trimethylsilyl)phosphine: A novel route to indium-phosphide. *J. Chem. Soc., Chem. Commun.* **1989**, 359−360.

55. Allen, P. M.; Walker, B. J.; Bawendi, M. G. Mechanistic Insights into the Formation of InP Quantum Dots. *Angew. Chem., Int. Ed.* **2010**, *49*, 760−762.

56. Yan, P.; Xie, Y.; Wang, W.; Liu, F.; Qian, Y. A-low temperature route to InP nanocrystals. *J. Mater. Chem.* **1999**, *9*, 1831−1833.

57. Carenco, S.; Demange, M.; Shi, J.; Boissierè, C.; Sanchez, C.; Le Floch, P. Le; Mézailles, N. White phosphorus and metal nanoparticles: A versatile route to metal phosphide nanoparticles. *Chem. Commun.* **2010**, *46*, 5578−5580.

58. Mellor, J. W. A Comprehensive Treatise on Inorganic and Theoretical Chemistry; Longmans: London, 1971.

59. Donohue, J. The Structure of the Elements; Wiley: New York, 1974.

60. Corbridge, D. E. C. Phosphorus: Chemistry, Biochemistry and Technology, 6th ed.; CRC Press: Boca Raton, FL, USA, 2013.

61. Song, W.-S.; Lee, H- S.; Lee, J. C.; Jang, D. S.; Choi, Y.; Choi, M.; Yang, H. Amine-Derived Synthetic Approach to Color-Tunable InP/ZnS Quantum Dots with High Fluorescent Qualities. *J. Nanopart. Res.* **2013**, *15*, 1750−1759.

62. Tessier, M. D.; Dupont, D.; De Nolf, K.; De Roo, J.; Hens, Z. Economic and Size-Tunable Synthesis of InP/ZnE (E= S, Se) Colloidal Quantum Dots. *Chem. Mater.* **2015**, *27*, 4893−4898.

63. Kim, K.; Yoo, D.; Choi, H.; Tamang, S.; Ko, J. H.; Kim, S.; Kim, Y. H.; Jeong, S. Halide−Amine Co-Passivated Indium Phosphide Colloidal Quantum Dots in Tetrahedral Shape. *Angew. Chem.* **2016**, *128*, 3778−3782.

64. Xi, L.; Cho, D.-Y.; Besmehn, A.; Duchamp, M.; Gr ützmacher, D.; Lam, Y. M.; Kardynał, B. E. Effect of Zinc Incorporation on the Performance of Red Light Emitting InP Core Nanocrystals. *Inorg. Chem.* **2016**, *55*, 8381−8386.

65. Xu, S.; Ziegler, J.; Nann, T. Rapid Synthesis of Highly Luminescent InP and InP/ZnS Nanocrystals. *J. Mater. Chem.* **2008**, *18*, 2653−2656.

66. Altıntas, Y.; Talpur, M. Y.; Ünlü, M.; Mutlugun, E. Highly Efficient Cd-Free Alloyed Core/Shell Quantum Dots with Optimized Precursor Concentrations. *J. Phys. Chem. C* **2016**, *120*, 7885−7892.

67. Klimov, V. I.; McBranch, D. W.; Leatherdale, C. A.; Bawendi, M. G. Electron and hole relaxation pathways in semiconductor quantum dots. *Phys. Rev. B: Condens. Matter Mater. Phys.* **1999**, *60*, 13740.

68. Wang, X.; Qu, L.; Zhang, J.; Peng, X.; Xiao, M. Surface-related emission in highly luminescent CdSe quantum dots. *Nano Lett.* **2003**, *3*, 1103−1106.

69. Kim, S.; Kim, T.; Kang, M.; Kwak, S. K.; Yoo, T. W.; Park, L. S.; Yang, I.; Hwang, S.; Lee, J. E.; Kim, S. K.; et al. Highly Luminescent InP/GaP/ZnS Nanocrystals and Their Application to White Light-Emitting Diodes. *J. Am. Chem. Soc.* **2012**, *134*, 3804−3809.

70. Li, L.; Reiss, P. One-pot synthesis of highly luminescent InP/ZnS nanocrystals without

precursor injection. *J. Am. Chem. Soc.* **2008**, *130*, 11588−11589.

71. Pietra, F.; De Trizio, L.; Hoekstra, A. W.; Renaud, N.; Prato, M.; Grozema, F. C.; Baesjou, P. J.; Koole, R.; Manna, L.; Houtepen, A. J. Tuning the Lattice Parameter of InxZnyP for Highly Luminescent Lattice-Matched Core/Shell Quantum Dots. *ACS Nano* **2016**, *10*, 4754−4762.

72. Luo, Y.-R.; Kerr, J. A. Bond dissociation energies. CRC Handbook of Chemistry and Physics, Vol. 87; CRC Press: Boca Raton, FL, USA, 2007.

73. Nose, K.; Fujita, H.; Omata, T.; Otsuka-Yao-Matsuo, S.; Nakamura, H.; Maeda, H. Chemical Role of Amines in the Colloidal Synthesis of CdSe Quantum Dots and Their Luminescence Properties. *J. Lumin.* **2007**, *126*, 21−26.

74. Fichera, M. A.; Braun, U.; Schartel, B.; Sturm, H.; Knoll, U.; Jäger, C. Solid-state NMR investigations of the pyrolysis and thermo-oxidative decomposition products of a polystyrene/red phosphorus/magnesium hydroxide system. *J. Anal. Appl. Pyrolysis* **2007**, *78*, 378.

75. Gary, D. C.; Cossairt, B. M. Role of Acid in Precursor Conversion During InP Quantum Dot Synthesis. *Chem. Mater.* **2013**, *25*, 2463−2469.

76. Gary, D. C.; Terban, M. W.; Billinge, S. J.; Cossairt, B. M. Two-Step Nucleation and Growth of InP Quantum Dots via Magic-Sized Cluster Intermediates. *Chem. Mater.* **2015**, *27*, 1432−1441.

77. Tessier, M. D.; De Nolf, K.; Dupont, D.; Sinnaeve, D.; De Roo, J.; Hens, Z. Aminophosphines: A Double Role in the Synthesis of Colloidal Indium Phosphide Quantum Dots. *J. Am. Chem. Soc.* **2016**, *138*, 5923−5929.

78. Buffard, A.; Dreyfuss, S.; Nadal, B.; Heuclin, H.; Xu, X.; Patriarche, G.; Mézailles, N.; Dubertret, B. Mechanistic Insight and Optimization of InP Nanocrystals Synthesized with Aminophosphines. *Chem. Mater.* **2016**, *28*, 5925−5934.

79. Lauth, J.; Strupeit, T.; Kornowski, A.; Weller, H. A Transmetalation Route for Colloidal GaAs Nanocrystals and Addi-tional III−V Semiconductor Materials. *Chem. Mater.* **2013**, *25*, 1377−1383.

80. Park, J.; Koo, B.; Yoon, K. Y.; Hwang, Y.; Kang, M.; Park, J. G.; Hyeon, T. Generalized Synthesis of Metal Phosphide Nanorods via Thermal Decomposition of Continuously Delivered Metal−Phosphine Complexes Using a Syringe Pump. *J. Am. Chem. Soc.* **2005**, *127*, 8433−8440.